5-2014

Production of Nuclear Debris Surrogates for Forensic Methods Development

Joshua James Molgaard
University of Tennessee - Knoxville, jmolgaar@utk.edu

To the Graduate Council:

I am submitting herewith a thesis written by Joshua James Molgaard entitled "Production of Nuclear Debris Surrogates for Forensic Methods Development." I have examined the final electronic copy of this thesis for form and content and recommend that it be accepted in partial fulfillment of the requirements for the degree of Master of Science, with a major in Nuclear Engineering.

Howard L. Hall, Major Professor

We have read this thesis and recommend its acceptance:

Lawrence H. Heilbronn, Guillermo Ivan Maldonado

Accepted for the Council:
Carolyn R. Hodges

Vice Provost and Dean of the Graduate School

(Original signatures are on file with official student records.)

Production of Nuclear Debris Surrogates for Forensic Methods Development

A Thesis Presented for the

Master of Science

Degree

The University of Tennessee, Knoxville

Joshua James Molgaard

May 2014

To my wife, Allison, and my two sons, Austin and Dillon. Thank you for your love, patience and continued support.

Acknowledgements

I would like to thank my advisor, Dr. Howard Hall, for providing the motivation and the resources to accomplish this work. I would also like to thank LTC Sam Willmon and MAJ Ed Peskie for reminding me daily about my real job. Support and practical assistance from Dr. John Auxier II was invaluable - his presence in the lab and personal involvement in this project improved the quality of the results. Thanks also to Dr. Joe Birdwell, Process Engineering Research (PER) Group Leader at the Oak Ridge National Laboratory (ORNL), for providing expertise to support concurrent and future work. Dr. Vince Jodoin's assistance in obtaining and learning to use the Fallout Analysis Tool (FAT) and DELFIC (DoD Fallout Prediction System) Fallout Planning Tool (FPT) is also greatly appreciated. The contributions of my undergraduate research assistant, C.J. Oldham, were also essential to the completion of this project - his dedication and hard work should not go unrecognized. I am grateful to Matthew Cook for regular assistance with computer issues and for assisting with the collection of gamma-ray spectrum data for trinitite and synthetic nuclear melt glass samples. Discussions with David Glasgow at the High Flux Isotope Reactor (HFIR) regarding plans for sample activation proved immensely helpful. I would also like to acknowledge the contributions of Stephan Young and Greg Jones who assisted with Scanning Electron Microscope (SEM) imaging which was essential for the success of my first peer reviewed publication. Finally, and most importantly, I must thank God for the opportunity and the ability to study and endeavor to comprehend His universe.

"It is not possible to be a scientist unless you believe that the knowledge of the world, and the power which this gives, is a thing which is of intrinsic value to humanity, and that you are using it to help in the spread of knowledge, and are willing to take the consequences." - Robert Oppenheimer (Quoted in "The Making of the Atomic Bomb" by Richard Rhodes)

Abstract

A novel method for producing synthetic debris similar to the melt glass produced by nuclear surface testing is demonstrated. Melt glass from the first nuclear weapon test (commonly referred to as trinitite) is used as the benchmark for this study. These surrogates can be used to simulate a variety of scenarios and will serve as a tool for developing and validating forensic analysis methods.

The ultimate goal is to provide the nuclear forensics community with a robust method to supply realistic yet non-sensitive surrogate materials simulating a variety of detonation scenarios. This work will also allow for the development of more analytical techniques for investigating post-detonation material.

Table of Contents

List of Tables

List of Figures

Chapter 1

Introduction

This section will introduce the topic of post-detonation nuclear forensics and discuss the importance of accurate and timely analysis techniques. The necessity of producing realistic debris surrogates will also be explained here.

1.1 The Need for Nuclear Forensics Capabilities

Preventing the illicit use of nuclear material is one of the major challenges of the modern era. The threat of proliferation and nuclear terrorism is a continued and growing concern. While disagreements persist regarding the likelihood of a nuclear attack by terrorists, and arguably the probability is low, the catastrophic consequences of such an event do not allow for complacency. In addition, the threat of proliferation or illicit use by rogue nations persists and must not be ignored.

The threat of nuclear terrorism has been recognized by congress and was the primary motivation for the passage of the Nuclear Forensics and Attribution Act [1]. This act called for the development of a credible capability for identifying sources of nuclear material used in a terrorist act, and also acknowledged the challenge presented by the dwindling number of radiochemical programs and facilities in the United States. The Domestic Nuclear Detection Office (DNDO) was tasked to establish

the National Technical Nuclear Forensics Center and the National Nuclear Forensics Expertise Development Program to foster enduring academic pathways for students in the fields of radiochemistry, geochemistry, nuclear physics, nuclear engineering, materials science, and analytical chemistry [1].

The Radiochemistry Center of Excellence (RCoE) established at the University of Tennessee (UT) and funded by the National Nuclear Security Administration (NNSA) seeks to fill the academic gap and meet the challenges identified in the Nuclear Forensics Attribution Act. One of the primary focus areas of the RCoE is the development of improved radiochemical separation and analysis methods with the goal of reducing the time required for accurate post-detonation analysis.

1.2 The Need for Nuclear Debris Surrogates for Forensic Methods Development

The National Center for Nuclear Security (NCNS) defines nuclear forensics as "the collection, characterization, analysis, and evaluation of nuclear or radiological materials, samples, devices, constituent parts, output signals, debris, and other related items resulting from the illicit use or intended use of radiological or nuclear material." The debris mentioned here refers to nuclear fallout or nuclear melt glass such as that deposited on the ground at the Nevada National Security Site (NNSS) by several legacy surface detonations [2]. The production of synthetic debris is the subject of this thesis.

The ultimate goal of this research project is the development of nuclear debris surrogates in the form of bulk sample media which contain fission product, activation product, and fission fuel signatures for testing and evaluation of forensic methodologies. The development of these debris surrogates is important for several reasons. First, the debris samples from nuclear tests do not contain many of the short lived radionuclides which will be present in fresh debris from a nuclear explosion. Second,

existing debris samples are often not available to the academic community. And lastly, because nuclear testing was not conducted in urban areas, there are no debris samples containing unique signatures from an urban detonation. A capability for producing realistic debris samples which can be made to simulate a variety of specific scenarios will prove an invaluable tool for validating analysis methods.

Chapter 2

Production of Nuclear Debris

2.1 Nuclear Explosion Categories

Nuclear testing has been conducted in a variety of environments, however, a nearly infinite number of explosive scenarios can be imagined. A defining parameter is the height (or depth) at which the detonation occurs. The term Height-of-Burst (HOB) is used for detonations above ground while the term Depth-of-Burst (DOB) refers to subsurface or underwater detonations. In general, nuclear explosions fall into one of four basic categories: Airburst, Surface Burst, Subsurface Burst or Underwater Burst. Each of these categories will be discussed briefly, however, only surface and subsurface bursts are of interest for this study.

2.1.1 Airburst

A nuclear detonation with a HOB such that the resulting fireball does not touch the ground is defined as an airburst [3]. No soil is displaced in an airburst and the debris originates from the device alone. This debris will be dispersed over a large area as nuclear fallout. Because no melt glass is produced by an airburst this category will not be examined here. Subcategories, based on HOB, include high altitude bursts and space shots which are sometimes treated separately because of their unique effects.

More information on these and other types of nuclear explosions can be found in the Nuclear Weapons Archive (http://nuclearweaponarchive.org).

2.1.2 Surface Burst

A surface burst is defined as any nuclear explosion which originates on or near the surface of the earth and results in the displacement, melting and even vaporization of local soil [3]. This definition would include the numerous tests which were traditionally classified as tower shots. Surface bursts are of particular interest for this present study due to the substantial production of nuclear melt glass and relevance to the field of post-detonation nuclear forensics.

2.1.3 Subsurface Burst

When a device is detonated underground the resulting explosion is referred to as a subsurface burst. Tunnel shots are included in this category. The DOB and weapon yield determine whether or not the explosion will be contained. A shallow subsurface burst will produce a crater and debris similar to a surface burst. The degree to which a subsurface burst is contained will impact the physics of the explosion [4]. A fully contained subsurface burst is an interesting scenario which will be simulated in future studies. While the threat of a deep underground explosion with malicious purposes is almost non-existent, extensive underground testing was conducted at the Nevada National Security Site (NNSS) and data from these tests is available for validation [5] [4] [6].

2.1.4 Underwater Burst

An underwater burst, as the name implies, is the result of a detonation which occurs underwater. Testing was also conducted on barges and small islands or atolls where a large quantity of water was displaced. These tests comprise a unique category which will not be explored in this study. However, future studies will be suggested which

will expand surrogate debris production capabilities to include a variety of potential simulations. Improvised nuclear devices, urban detonations and underwater bursts will be of interest in the future.

2.2 Debris from Subsurface Bursts

For simplicity a fully contained subsurface burst will be described here. In this case a cavity is formed and the pressure inside the cavity is initially balanced against the lithostatic pressure (stress imposed on the cavity ceiling by the weight of the overlying material). The molten material forms a puddle at the bottom of the cavity and the gases in the cavity begin to condense. The pressure eventually drops below the lithostatic pressure and the cavity collapses on itself. This collapse causes large rock fragments to be mixed with the partially molten glass at the bottom of the cavity. The intense energy of the explosion causes shock melting followed by rapid quenching and mixing with rock fragments, leading to a very heterogeneous melt glass [4]. In this scenario the debris is entirely preserved, with the exception of any gases that escape following cavity collapse. Some volatile fission products may be lost (those which do not condense prior to cavity collapse) and the fraction lost will depend on the time of collapse (ranging from seconds to days, depending on the depth of burst, weapon yield, and stability of the host rock formation). Refractory fission products will be mixed throughout the volume of the melt glass puddle. Volatile fission products that survive will condense later in the cooling process and thus be concentrated on the surface of the melt glass. It is estimated that 700 metric tons of melt glass is produced per kiloton of yield in an underground explosion [7].

Debris from a fully contained subsurface burst is perhaps the easiest to reproduce in a laboratory. The fact that such debris is entirely localized eliminates the need to consider large scale fractionation of the fallout field (as with a surface burst). If cavity collapse is not immediate the molten debris will cool more gradually than surface debris. While the high pressure inside the cavity is not easily re-created

in a laboratory, the shock melting followed by gradual cooling (or rapid cooling) is a fairly straightforward process. In fact, fractionation within a sample may occur during gradual cooling in a lab furnace in much the same as it would in the cavity of a subsurface nuclear explosion. Unfortunately, this scenario is not especially useful from a forensics standpoint as the only benefit of reproducing such debris would be to validate the debris making process. It is highly unlikely that a nuclear attack would ever be staged in such a way that the debris would be fully contained underground. A surface detonation is far more feasible and would likely occur in a population center with a complex network of buildings and materials making the composition of the resulting debris very difficult to predict. This is the challenge that will begin to be addressed in the remainder of this thesis.

2.3 Prompt Local Debris from Surface Bursts

Surface explosions produce large quantities of debris which contain materials from the weapon and the surrounding environment. Some debris is carried away from ground zero in particulate form and is classified as fallout. This study focuses on the production of prompt debris near ground zero (nuclear melt glass). The first production of nuclear melt glass occurred during the Trinity test (a surface burst) on July 16th, 1945. Heat from the initial burst of thermal energy promptly fused the surrounding sand and subsequent heating by the fireball produced a smooth glassy surface on top of the trinitite lake. A large quantity of sand (and other material) was also scooped up by the fireball and heavier particles began to rain back down within a few seconds [8].

The average thickness of the trinitite lake was about 0.5 cm [8]. The lake was approximately circular with a radius of about 500 m [9] as shown in figure 2.1.

Trinitite contains glass formed from feldspar and clay as well as silica glass formed by the fusing of quartz in the sand [10]. The melt glass closest to ground zero contains an abundance of green trinitite [11] which is glassy and vesicular (see Figure 2.2).

SEM analysis shows variability in the glass composition (Figure 2.3). Similar types of debris have been produced by numerous tests at the Nevada National Security Site (previously known as the Nevada Test Site).

The initial goal of this project is to produce nuclear melt glass surrogates similar to those produced by surface testing in desert environments. The debris formulations will eventually be modified to include ingredients characteristic of urban environments and simulating a range of explosive scenarios.

2.4 Debris from Nuclear Testing

As previously mentioned, a significant quantity of surface debris exists from the nuclear testing era, however, these debris samples are not available to the general public or academic institutions. The only debris samples which remain unclassified are those taken from the first nuclear test (Trinity) conducted near Socorro, New

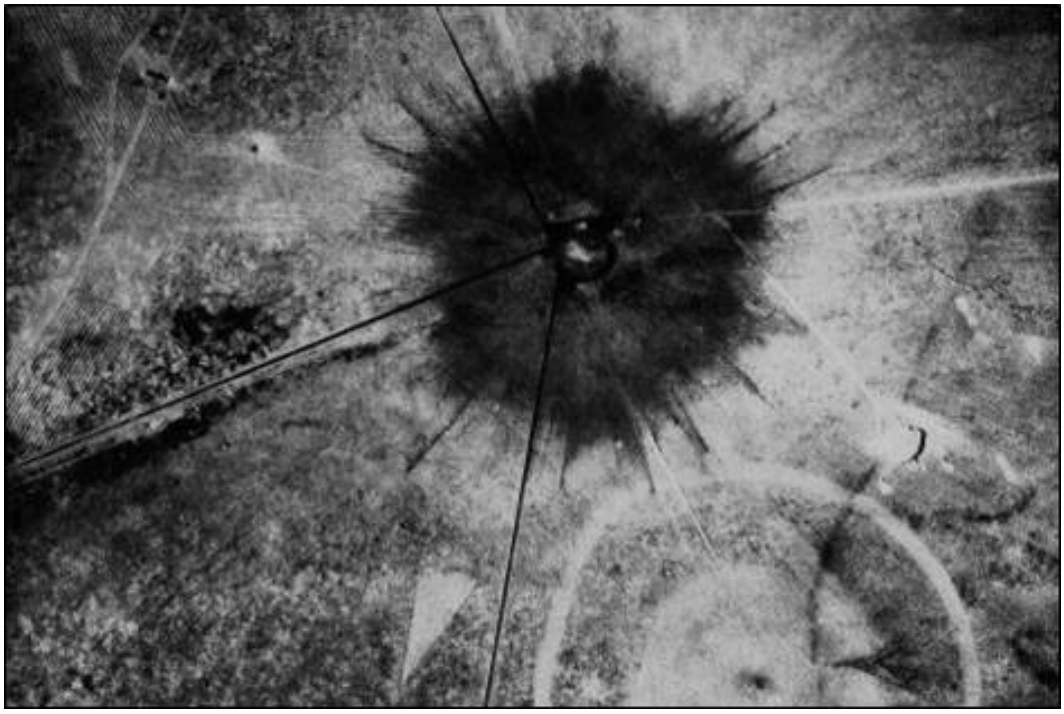

Figure 2.1: Aerial photo of the Trinity crater an trinitite lake (from the Nuclear Weapon Archive - nuclearweaponarchive.org).

Mexico at the White Sands Missile Range. Trinitite is available from various mineral collectors. For this present work several samples of trinitite were purchased from the Mineralogical Research Company (http://www.minresco.com) based in San Jose, California.

The first and primary task of this research effort is to produce a sample of synthetic trinitite which displays the correct chemical, physical and morphological characteristics. Synthetic samples can be compared to actual trinitite using Scanning Electron Microscopy (SEM), Energy Dispersive X-Ray Spectroscopy (EDS), Powder X-Ray Diffraction (P-XRD) and qualitative analysis. Activated samples can also be compared to trinitite via gamma spectroscopy and alpha spectroscopy (correcting for age differences).

Figure 2.2: Samples of green trinitite (from [11]).

2.5 Modeling

The Fallout Analysis Tool (FAT) was recently added to the Standardized Computer Analysis for Licensing Evaluation (SCALE) code system [12] [13] as a limited distribution software for predicting the composition of fallout from a nuclear detonation. FAT allows a user to define a source term by inputing fuel types (Uranium or Plutonium) and quantities along with isotopic breakdown and compositions of carrier materials (e.g. soil constituents). The user also chooses the weapon yield and cross section libraries. FAT uses SCALE 6.1 to simulate a reactor run at high power for a very short duration (1 microsecond). The Oak Ridge Isotope Generation and Depletion (ORIGEN) code [12] is then employed to decay the activation products, fission products and actinides as requested by the user. Radioisotopes can be sorted by mass, activity, number of atoms, atomic number, mass number, half-life, or decay

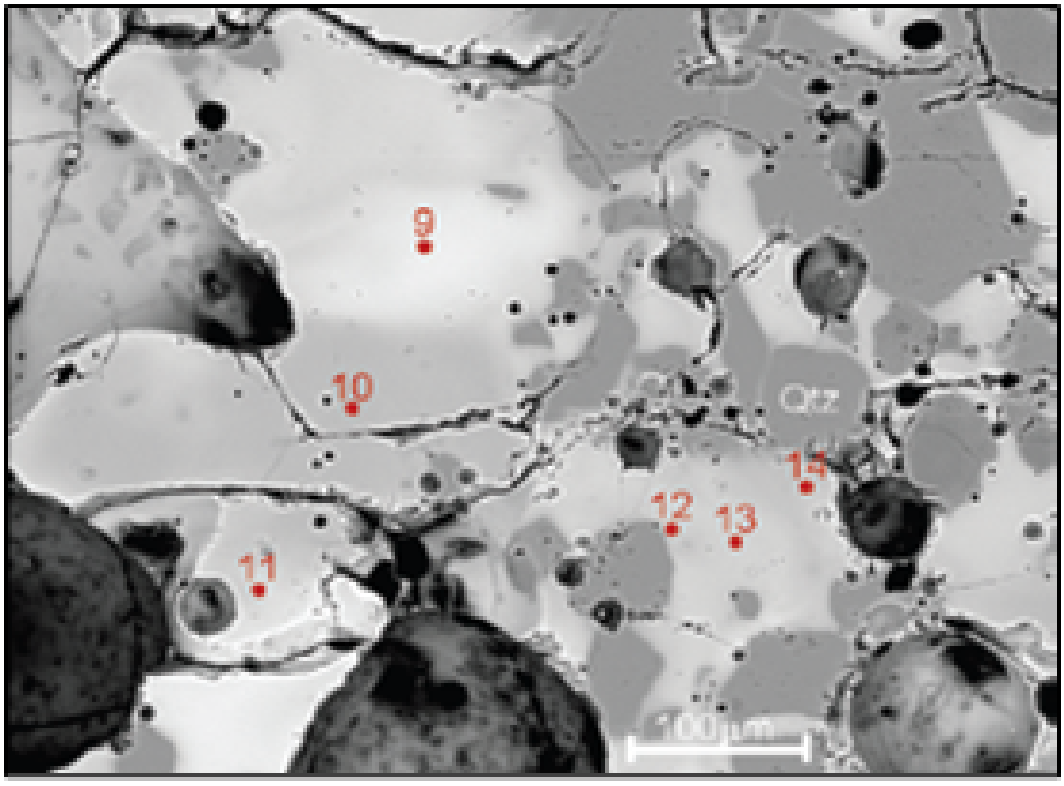

Figure 2.3: SEM BSE image of trinitite sample (from [11]). The bright spots indicate areas of high Iron and/or Calcium concentration.

constant. Tables can be constructed containing all radioisotopes or specific categories (actinides, fission products or activation products). Concentration or activity of any isotope can be plotted over time [13]. This tool was used to predict (prior to irradiation) the composition and radioactivity of various activated samples.

One purpose of such modeling is to predict the radioactive hazard associated with irradiation of debris samples (e.g. at HFIR). This may influence irradiation methods as well as post-irradiation handling and analysis procedures. Another purpose of modeling is to estimate the neutronics requirements for producing accurate debris surrogates. FAT allows the user to choose an initial neutron library with a thermal spectrum, fast fission spectrum or high energy spectrum (greater than 14 MeV). In general, a fast fission library is preferred for nuclear fallout calculations [13]. However, the neutron energy spectrum available in the pneumatic tube system at HFIR is predominately thermal. In reality, the fission spectrum characteristic of a given nuclear weapon will likely fall between these two extremes. Hand calculations can be performed to predict the concentration and activity of specific radioisotopes (using, for example, the Watt fission spectrum or an empirical formula) and these results can be compared to models using different neutron libraries. In this way the optimal irradiation parameters can be determined or, alternatively, the chemistry of the synthetic debris sample can be modified to compensate for neutronic disparities.

The fission curves for ^{235}U and ^{239}Pu with both thermal and fast fission neutron spectra are compared in figure 2.4. These curves were generated using FAT to model the irradiation of a 2 gram sample of trinitite containing 2.45 milligrams of natural uranium. Of particular significance are the curves for fast fission of ^{235}U and fast fission of ^{239}Pu as these will characterize the majority of nuclear devices. Differences between ^{235}U and ^{239}Pu fission yields provide key forensic signatures and so it is important to preserve these differences within any surrogate debris material.

Figure 2.5 shows the differences between thermal and fast fission of ^{235}U compared to the differences between fast fission of ^{239}Pu and fast fission of ^{235}U. The greatest overlap occurs for mass chains 85-95 and 101-109 suggesting that special attention

must be given to isotopes with A=85-95 and A=101-109 when developing surrogate debris. These mass chains are represented graphically in figures 2.6 through 2.8. Refractory isotopes are represented with red letters while volatile isotopes are shown in blue. In this case refractory isotopes are defined as those with melting temperatures greater than 2000 K and volatiles are those with melting temperatures lower than 2000 K (solidification temperature of silicon dioxide). The cumulative yields of each fission product are also indicated (in percent per fission). The cumulative yields are based on the fast fission of ^{235}U and include contributions from decay of parent fission products.

Nuclear melt glass is produced close to ground zero and is expected to be rich in refractory fission products. The volatile fission products will be preferentially carried away by winds and eventually deposited far from ground zero (fallout). For surrogate melt glasses where fission products are generated by thermal neutron irradiation

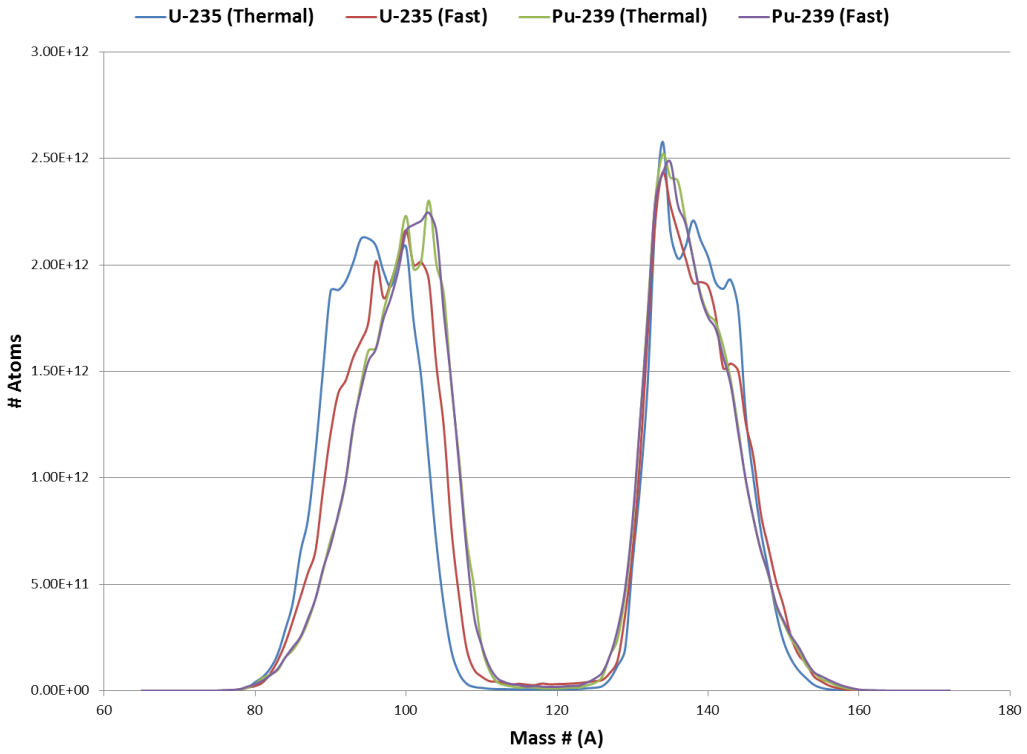

Figure 2.4: Fission curves generated by the Fallout Analysis Tool.

it may be necessary to "enrich" samples with refractory members of mass chains 85-95 and 101-109 which have substantial cumulative fission yields. This may be accomplished by adjusting the chemistry of the matrix to include stable members of the appropriate mass chains. Stable isotopes will be transmuted by neutron capture during irradiation to produce artificial fission products.

From figure 2.6 it is evident that the only refractory fission product of mass 85-88 with a substantial yield is Strontium (in particular ^{87}Sr and ^{88}Sr). Both ^{87}Sr and ^{88}Sr are stable and can be easily incorporated into synthetic melt glass samples prior to irradiation. Small excesses (in the picogram range) may be included to allow for activation by neutron capture, to produce heavier isotopes of strontium.

Mass chains 89-92 include the refractory fission products strontium, yttrium and zirconium. ^{89}Sr has a half-life of 50.53 days and can be produced by neutron capture on ^{88}Sr. ^{90}Sr is important because of its relatively long half-life (28.79 years) and

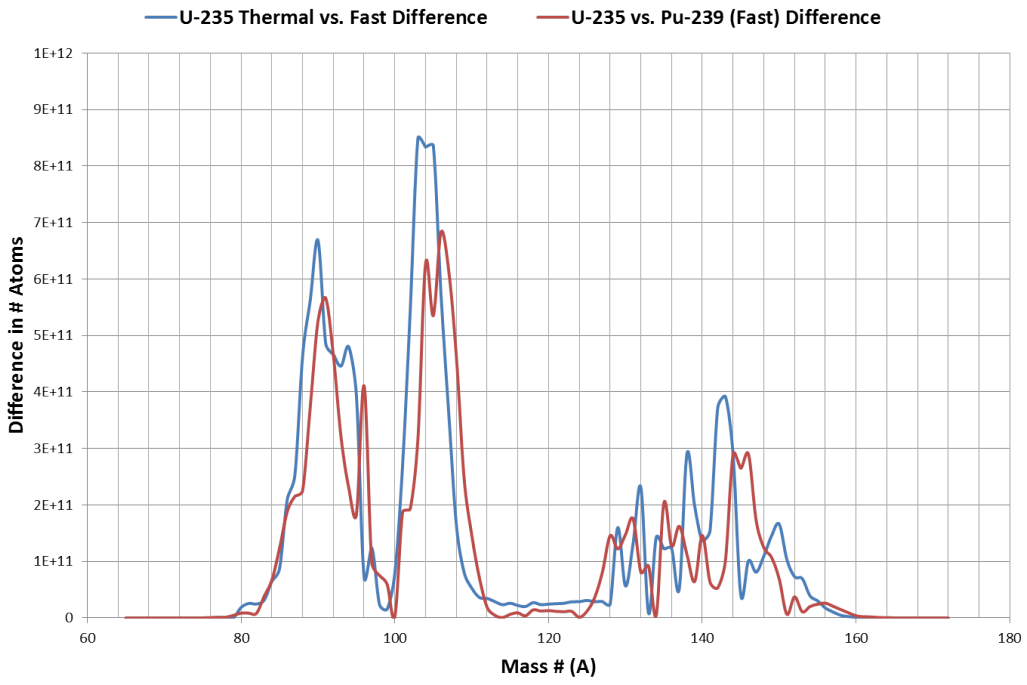

Figure 2.5: Differences in fission yields for ^{235}U (fast and thermal) compared to differences for fast fission (^{235}U and ^{239}Pu).

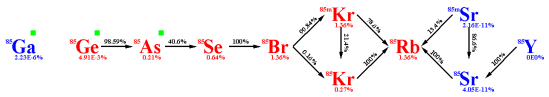

(a) Mass Chain 85

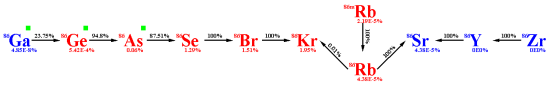

(b) Mass Chain 86

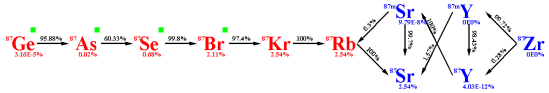

(c) Mass Chain 87

(d) Mass Chain 88

Figure 2.6: Mass Chains 85-88.

substantial fission yield. ^{91}Sr and ^{92}Sr are relatively short lived radioisotopes (half-lives of 9.63 hours and 2.71 hours respectively) but with substantial yields. ^{89}Y is stable while ^{90}Y and ^{91}Y have half-lives of 2.67 and 58.51 days respectively. ^{92}Y has a rather high fission yield but a half-life of only 3.54 hours. ^{90}Zr, ^{91}Zr, and ^{92}Zr are stable.

Mass chains 93-95 also include isotopes of strontium, yttrium, and zirconium as well as niobium. ^{93}Sr, ^{93}Y, ^{93}Zr and ^{93}Nb all have cumulative fission yields over 6 percent per fission. ^{93}Sr is rather short-lived with a half-life of 7.42 minutes, ^{93}Y has

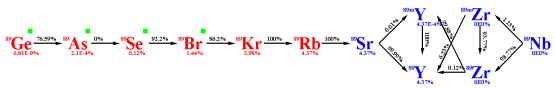

(a) Mass Chain 89

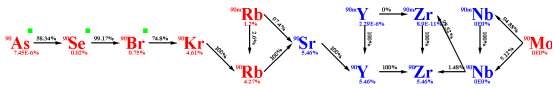

(b) Mass Chain 90

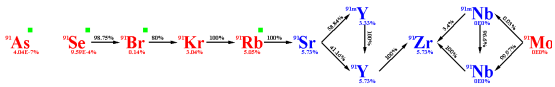

(c) Mass Chain 91

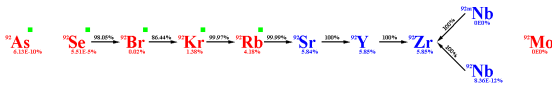

(d) Mass Chain 92

Figure 2.7: Mass Chains 89-92.

a half-life of 10.18 hours, and ^{93}Zr is long-lived with a half-life of 1.53 million years. ^{93}Nb is stable. The short-lived ^{93m}Y has a 2.2 percent yield and a half-live of 0.82 seconds. ^{93m}Nb has a yield of 5.94 percent and a half-life of 16.13 years. ^{94}Sr and ^{95}Sr with half-lives of 1.26 minutes and 23.9 seconds respectively will contribute to the early activity of fresh debris. ^{94}Y with a half-life of 18.7 minutes and ^{95}Y with a half-life of 10.3 minutes both have substantial fission yields as do ^{94}Zr and ^{95}Zr. ^{94}Zr is stable while ^{9}Zr has a half-life of 64.03 days. The yield of ^{94}Nb is negligible while ^{95}Nb has a high yield and a half-life of 34.99 days.

(a) Mass Chain 93

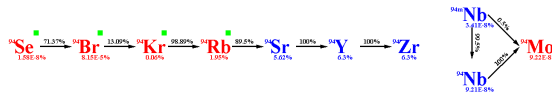

(b) Mass Chain 94

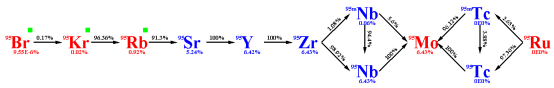

(c) Mass Chain 95

Figure 2.8: Mass Chains 93-95.

It is evident that nuclear melt glass will be rich in isotopes of strontium, yttrium, zirconium and niobium and these species lie in a mass range that is sensitive to fuel type and neutron energy spectrum. In general, fission yields in this mass range are higher for thermal fission of ^{235}U than for fast. Since uranium will be the primary fuel used for this study and activation will be accomplished by thermal neutron irradiation (at HFIR) it is desirable to design an experimental method that will artificially adjust the fission curve to more closely resemble that of a fission spectrum device.

FAT models were developed to predict the composition of a 2-g sample of nuclear melt glass containing approximately 10^{12} fissions. The masses of selected fission products in this notional sample were compared for both fast and thermal neutron spectra. In the case of strontium isotopes the differences for $^{85-88}Sr$ were practically negligible (less than a 10^{-15} g difference). For $^{89-95}Sr$ the differences ranged from approximately 0.3 to 26 picograms. The masses were always higher for thermal fission.

While it is difficult to reduce the quantity of fissions in a sample it may be possible to increase the yield artificially in another mass range (e.g. A=101-109) to alter the overall shape of the fission curve. If the relative concentrations of fission products are consistent with a fast fission spectrum the source of the fission products (some induced artificially) will be irrelevant for analysis purposes.

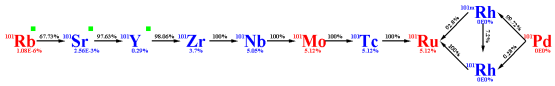

(a) Mass Chain 101

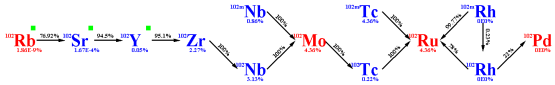

(b) Mass Chain 102

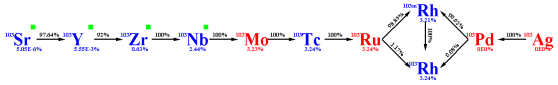

(c) Mass Chain 103

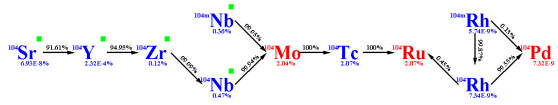

(d) Mass Chain 104

Figure 2.9: Mass Chains 101-104.

Looking at figures 2.9 and 2.10 and considering only refractory isotopes with substantial fission yields it can be seen that zirconium, niobium, technetium, and rhodium are the important elements in this mass range (A=101-108). The cumulative

fission yields for refractory members of mass chain 109 are very small (less than 0.1 percent per fission) so this data is not included here. Most of the refractory fission products in mass chains 101-108 are short-lived radioisotopes, including $^{101-102}Zr$ and $^{101-105}Nb$, all having half-lives shorter than 10 seconds. Isotopes of technetium have half-lives ranging from 5 seconds to 18 minutes. The exceptions are ^{103}Rh which is stable and ^{105}Rh which has a half-life of 1.47 days. Clearly these isotopes will be important for early analysis of fresh debris.

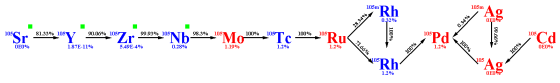

(a) Mass Chain 105

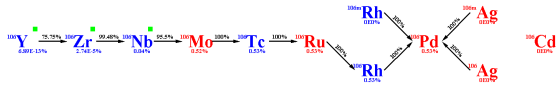

(b) Mass Chain 106

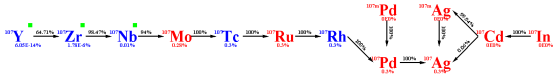

(c) Mass Chain 107

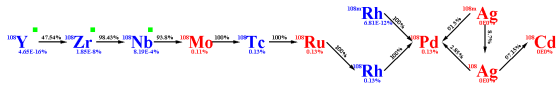

(d) Mass Chain 108

Figure 2.10: Mass Chains 105-108.

Although oxides of molybdenum, ruthenium, palladium and silver are considered volatile (compared to silicon dioxide) they are solids at room temperature and can

easily be added to a synthetic melt glass matrix prior to melting. Additionally, for these elements, the pure metals melt at higher temperatures then their oxides and although they are commonly assumed to appear as oxides within the nuclear cloud [13] the exact chemistry during cloud formation and dispersal is not well understood. Molybdenum, ruthenium, palladium, and silver have naturally occurring isotopes ranging in mass from 92 to 110 amu. Both stable and radioactive isotopes of these elements are embedded within the fission product mass chains 101-109. They are thus prime candidates to be used experimentally to enhance the apparent fission yields of these mass chains.

FAT was employed to model a 2-g sample of trinitite containing $1.93x10^{14}$ fissions (a 1 microsecond reactor run at 5579 MW) and small quantities of Mo, Ru, Rh, Pd, and Ag were added to alter the fission curve from A=85-110. The adjusted fission plus activation curve is shown in figure 2.11. Figures 2.11 through 2.15 were produced by counting both fission and activation products for each run.

Figure 2.12 shows the comparison between fast and thermal fission of ^{235}U when activation products are included in the curves. Figure 2.13 shows a similar comparison between thermal and adjusted thermal fission. The adjusted fission plus activation curve was generated by incorporating Mo (0.50 nanogram), Ru (2.30 nanogram), Rh (1.05 nanogram), Pd (1.00 nanogram), and Ag (1.00 nanogram) into the starting matrix.

Figure 2.14 compares a fast fission plus activation curve to the adjusted thermal curve shown in figure 2.13. Notice the similar shape of the curves between mass 85 and 110. Figure 2.15 also compares the adjusted thermal and fast fission plus activation curves, however, in this case the fast fission and activation yields have been increased by 15 percent. This demonstrates that, particularly for mass chains 85-110, an adjusted thermal fission curve may be comparable to a fast fission curve with 15 percent more total fissions.

The modeling results discussed here are promising and suggest that chemical adjustments can be made to surrogate debris samples which will lead to the simulation

of different neutron spectra once the samples are activated. Additional studies, including activation experiments, will be required to determine the reliability of this method.

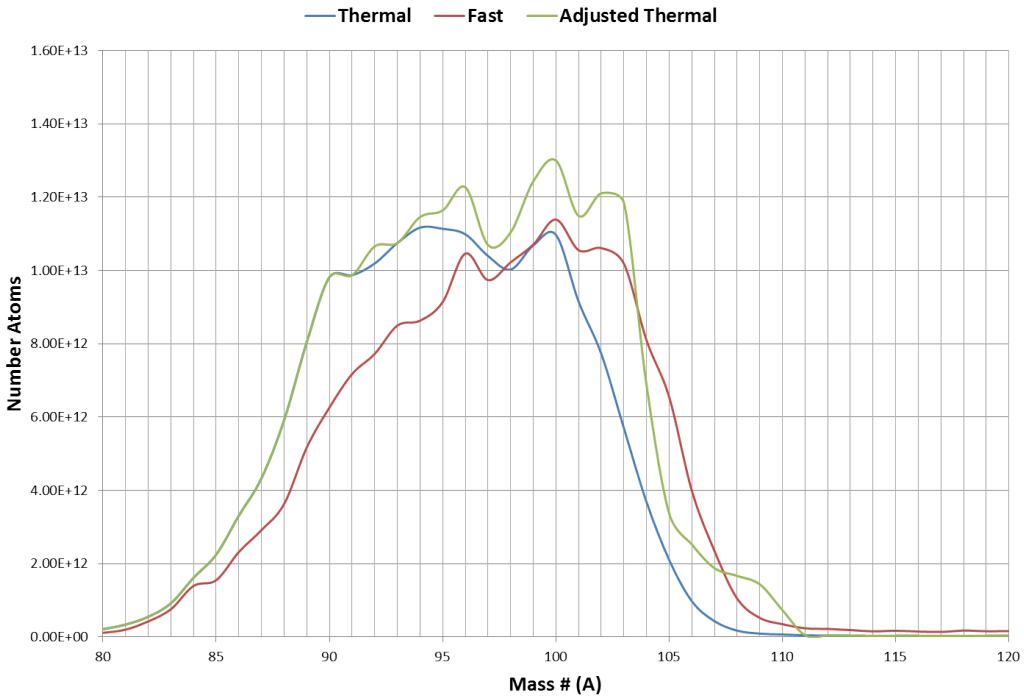

Figure 2.11: Adjusted fission plus activation curve for the thermal fission of ^{235}U compared to the same curves for fast and unaltered thermal fission.

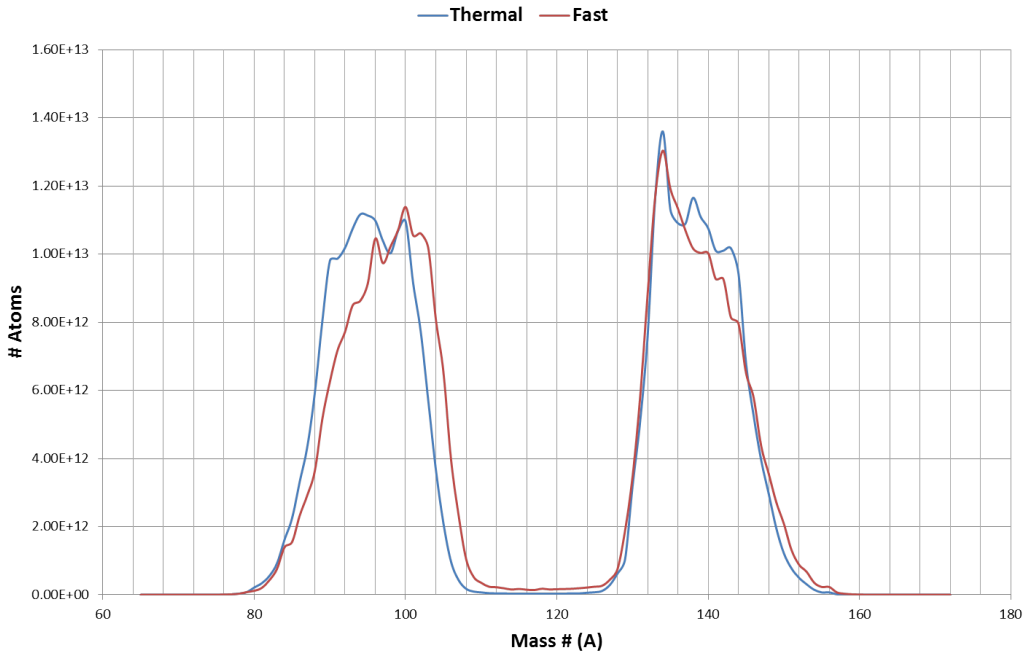

Figure 2.12: Fission plus activation curve for the thermal fission of ^{235}U compared to the same curve for fast fission.

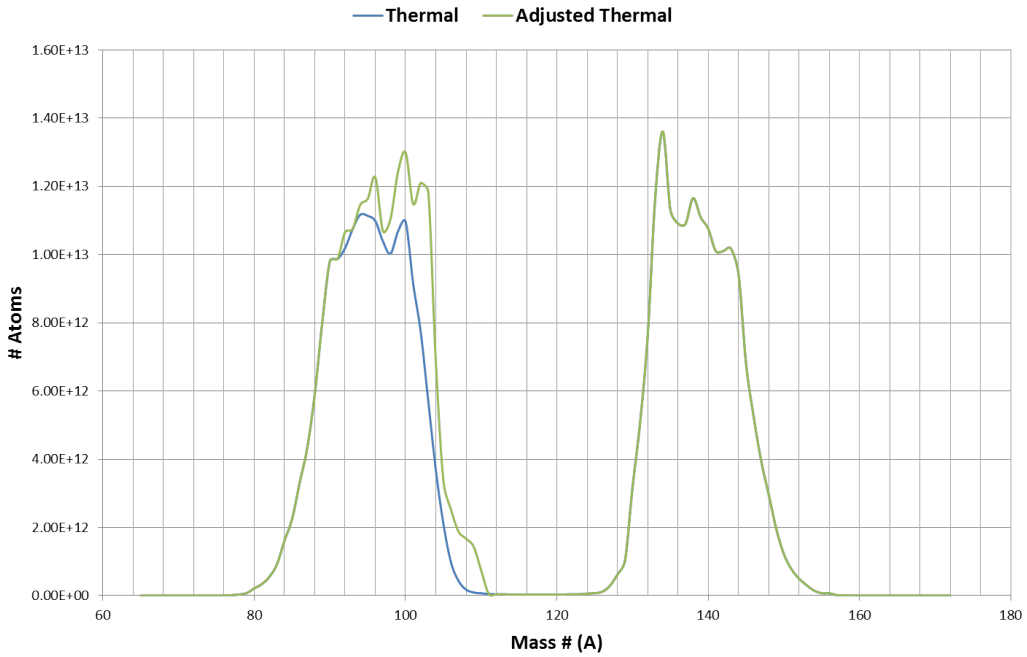

Figure 2.13: Adjusted fission plus activation curve for the thermal fission of ^{235}U compared to the same curve for unaltered thermal fission.

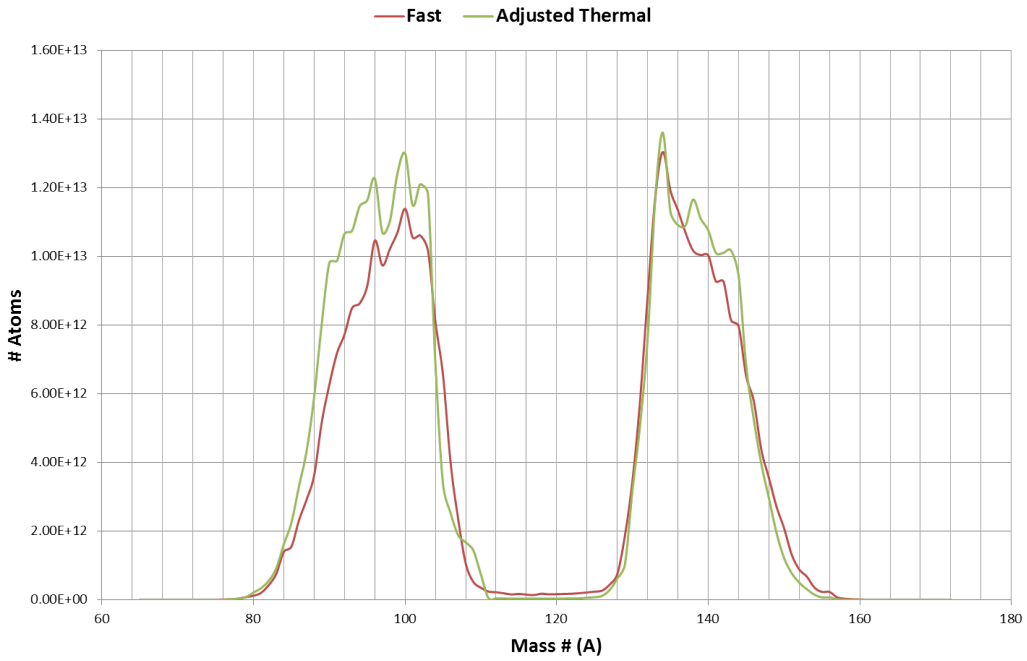

Figure 2.14: Adjusted fission plus activation curve for the thermal fission of ^{235}U compared to the same curve for unaltered fast fission.

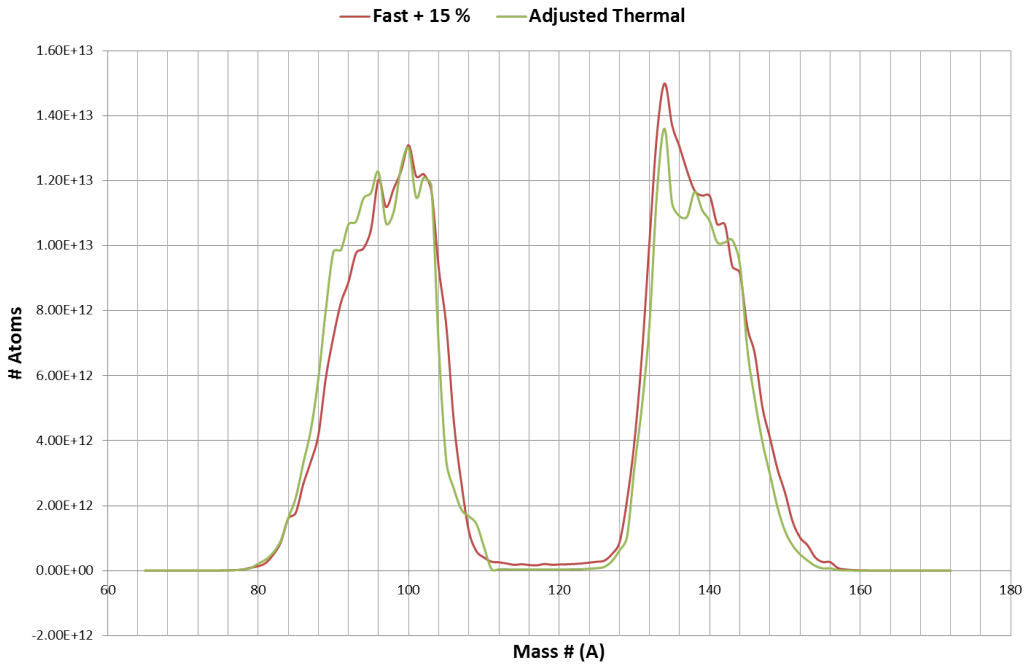

Figure 2.15: Adjusted fission plus activation curve for the thermal fission of ^{235}U compared to the unaltered fast fission curve shifted up 15 percent.

Chapter 3

Properties of Nuclear Melt Glass

3.1 Physical Properties

Physical properties of trinitite were examined and compared to the synthetic melt glass samples ultimately produced by this study. Published descriptions of trinitite were also considered along with photos and analysis of debris from underground and surface testing at the Nevada National Security site. The comparison between trinitite and synthetic surface debris is discussed in chapter 6.

3.1.1 Thickness

The trinitite samples purchased for analysis at the University of Tennessee were approximately 3-5 mm thick, on average. This thickness is consistent with previously published descriptions of trinitite [8] and is assumed to be typical for nuclear melt glass produced by surface detonations in desert environments. Melt glass from underground nuclear detonations will have a different physical form as it cools more gradually (compared to surface debris) and primarily collects in a puddle at the bottom of the test cavity [4].

Photos of underground melt glass samples reveal a wide range of fragment sizes and shapes. Large chunks of dark glass have been observed which contain some lighter

colored fragments. Thicknesses range from a few millimeters up to several centimeters and the shapes are irregular [4]. By contrast, the 8 trinitite samples observed at UT all have a flat geometry and fairly consistent thicknesses.

3.1.2 Texture and Color

The trinitite samples characterized for this study were all very similar and each was observed to have a smooth, glassy side and a somewhat rougher, grainier side. The smooth side is presumably the top layer which was exposed to the blast. The smoother side was generally light green in color but with a blotchy appearance. The rough side generally had a sandy, brown color. The samples were highly vesicular and brittle. Synthetic samples tended to be less brittle but shared many other textural features with trinitite (see chapter 6).

Underground melt glass samples have been observed to exhibit highly varied textures ranging from massive to highly vesicular. The color ranges from white to very dark (even with individual samples). The texture of the underground melt glass appears to be independent of the type of host rock and design of the weapon tested [4].

3.2 Chemical Properties

The key chemical properties of interest for this study are the elemental composition, compound structure and reactivity of nuclear melt glass. The composition is determined primarily by the carrier material with traces of nuclear fuel, fission products, and device components (including tamper material). The compound structure is affected by the rapid heating and cooling (vitrification). Melt glass is thus expected to be highly amorphous with few surviving crystalline structures. Reaction properties are important for analysis purposes (to determine appropriate chemical treatment and also for comparison to aged nuclear debris [5]).

3.2.1 Composition

The composition of nuclear melt glass will depend on the type of device and the environment in which it is detonated. For this study the composition of trinitite was examined and assumed to be fairly representative of debris from surface detonations in desert rural desert environments. Compositional estimates are discussed in greater detail in chapter 5.

Silicon will generally be the most prevalent element in any nuclear melt glass due to its high concentration in most soils. However, urban environments will likely include a significant amount of concrete which has a high lime (CaO) content. Metals and other structural materials will be more prevalent in urban areas as well. Future studies will examine the types of glasses produced with varied amounts of concrete, iron, aluminum, steel and window glass.

Initial composition will affect the resulting chemistry and morphology of the melt glass. For example, soil at the Trinity test site included quartz, microcline, albite, muscovite, actinolite, and calcite, however, quartz is the only mineral found in trinitite. The other minerals are believed to be completely melted [11]. Soil containing other minerals may lead to melt glass with a slightly different crystalline structure and morphology.

The focus of this current study is on the production of surface debris. Underground detonations may produce different results. In particular, melt glass from underground testing in the Pacific region will contain basalts with a typical silicon dioxide concentration of approximately 45 percent [6]. Synthetic melt glasses designed to simulate underground nuclear debris should be tested and compared to data from testing (both in Nevada and the Pacific region) in order to expand the production process for various compositions.

3.2.2 Reactivity

Melt glass is not highly reactive under normal conditions. Oxidation and corrosion are usually not a concern at short time scales (hours to days). However, alteration layers have been observed in aged underground melt glass [5]. Dissolution is possible and solutions have been prepared at UT using aqua regia to leach material from both trinitite and synthetic nuclear melt glass samples. Dissolution via saltwater of silica from underground nuclear melt glass in the Pacific region has been discussed elsewhere [6]. Reaction rates of approximately $1.6x10^{-3}g/m^2/day$ have been estimated for melt glasses with high basalt content (produced by underground testing in the Pacific region). For small samples this reaction rate is slow at timescales of interest for nuclear forensics analysis. The reaction rate is a function of temperature, pH and silica content [6]. Different carrier materials may dissolve more readily and this should be studied further. In particular, the reactivity of synthetic nuclear melt glass samples with a range of compositions should be compared to known data for various glass types. Preliminary results suggest that the synthetic samples produced for this study are similar to trinitite, in terms of their dissolution rates.

3.3 Morphology

Surface debris can take on several forms, as evidenced by examination of trinitite. Glass types include (1) pancake trinitite with a glassy top surface, (2) red trinitite containing copper, (3) green trinitite fragments, and (4) green trinitite beads and dumbbells [11]. Underground nuclear melt glasses are usually in the form of beads or fragments of various sizes, often incorporated with host rock [4]. All types of melt glass are found to be similar in terms of porosity, heterogeneity and structural defects. The morphology of trinitite is of primary interest for this current project.

3.3.1 Vitreous Nature

Trinitite is mostly amorphous. This has been verified by powder X-ray diffraction analysis (see chapter 6). Nuclear melt glass is believed to be formed by shock melting at very high temperatures followed by rapid cooling. This vitrification process is believed to occur within an 8-11 second time-frame after detonation [8]. The glassy nature of the trinitite samples observed at UT is consistent with this formation process. Analysis of synthetic melt glass samples have shown a similar degree of amorphousness, as will be discussed in chapter 6.

3.3.2 Microstructure

Nuclear melt glass is expected to be highly heterogeneous and contain approximately 30 percent voids [8]. Indeed, topographical and compositional heterogeneities have been observed in trinitite, even at the macroscopic level. Samples analyzed for this current work were observed to contain numerous voids of varying sizes when imaged with a Scanning Electron Microscope (SEM). Particulate inclusions were also seen at the 10-100 micron level. Evidence of surface eddies and flows have been reported previously [14] and these features were also observed via SEM analysis at UT. In addition, numerous cracks and surface defects can be clearly seen in SEM images of trinitite. Many such images are shown in chapter 6. Similar analysis of synthetic melt glass shows comparable features in the microstructure. A more detailed analysis of trinitite would likely reveal evidence of radiation damage in the glass.

3.3.3 Porosity

Trinitite has a varied but generally high degree of porosity. Underground nuclear melt glass is often highly porous as well [4]. The porosity of the synthetic melt glass samples was not quantified but was observed to be comparable to trinitite. The porosity and brittleness of the synthetic samples was largely dependent on melting time and temperature.

3.4 Radioactive Properties

The radioactivity of nuclear melt glass is perhaps its most useful attribute. The radionuclides which are detected will provide important information about the type of fuel, level of enrichment, weapon efficiency and nuclear yield.

3.4.1 Sources of Radioactivity

Nuclear melt glass is expected to contain actinides associated with the device fuel (e.g. plutonium, along with its daughters and activation products). If a natural uranium tamper is used (as in the Trinity test) the resulting nuclear melt glass will also contain uranium daughters and activation products. Fission products will also be trapped in the glass and intense neutron irradiation will product activation products in the carrier material (e.g. sand, concrete, metal). Thus, characterization of a samples radioactive properties may yield information about the fuel, tamper, device components, yield, efficiency of the weapon and carrier material (local environment).

3.4.2 Distribution of Radionuclides

Fractionation will affect the distribution of radionuclides in nuclear debris. In the case of an underground detonation refractory radionuclides will be largely incorporated within the glass which forms a puddle at the bottom of the cavity while the volatile radionuclides will tend to be distributed throughout the cavity-chimney system [6]. The this context refractory and volatile classifications are based on the boiling points of the radionuclides relative to the boiling point of the carrier material. In the case of a surface burst the melt glass which forms near ground zero will contain more refractory than volatile radionuclides. Conversely, the fallout which is carried farther from ground zero will contain a higher fraction of volatile radionuclides. The distribution within each particle and the distribution within the total debris/fallout field will be impacted by fractionation [15]. This applies to both air and surface bursts.

3.5 Analysis Methods

Accurate analysis techniques are important for validating experimental results. This section provides a brief overview of the analysis methods which may be employed to characterize synthetic samples and compare them to real samples (trinitite).

3.5.1 Microstructural Analysis

Nuclear melt glass is known to be heterogeneous and filled with defects, including cracks, bubbles and various inclusions [16] [14]. Some of these features will be observable on a macroscopic scale, however, the finer details will require microscopic analysis. Various forms of microscopy can be employed to analyze the elemental distributions, crystallographic structure and defects within the samples. Voids, grain boundaries and very small inclusions can be observed using electron microscopy. Several types of electron microscopy are discussed briefly in the succeeding paragraphs.

Scanning Electron Microscopy (SEM) is useful for obtaining topographical information and for analyzing the chemical composition near the surface of a sample [17]. SEM employs an electron source which is focused and then made to scan over the surface of a sample. Penetrating electrons undergo various types interactions with the sample material and these interactions lead to the production of three basic image types: Secondary Electron (SE) images, Backscattered Electron (BSE) images, and elemental X-ray maps. The SE images are especially useful for topographical analysis as the number of detectable secondary electrons depends on the slope of the surface [17]. BSE images can provide compositional information as well. Since the number of backscattered electrons increases with atomic number the heavy (high-Z) elements will produce stronger signals (brighter images) than the lighter elements. X-rays are also produced in the SEM process by the decay of excited atoms. These X-rays can be used, via Energy Dispersive Spectroscopy (EDS) to produce elemental maps that show the spacial distribution of the elements in a particular region on the surface of

a sample [17]. For this current work SEM analysis was performed using a LEO 1525 SEM and Zeiss Smart SEM software.

3.5.2 Chemical Analysis

An Inductively Coupled Plasma (ICP) produces exited atoms and ions in a Radio Frequency (RF) discharge. ICP Optical Emission Spectrometry (ICP-OES) takes advantage of the spontaneous emission of photons by these excited atoms and ions. The wavelengths of the characteristic photons can be used to determine the elemental composition of the sample. Soils and other solid samples can be dissolved to form liquid solutions or slurries which are converted to aerosols by a nebulizer. The aerosols are injected into the plasma where the extremely high temperatures will break down chemical bonds and produce ionization. ICP-OES is ideal for trace element analysis as most elements are detectable at concentration levels below 1 mg/L [18].

While the ICP-OES uses a diffraction grating to separate light emitted by the plasma into discrete component wavelengths, the ICP Mass Spectrometer (ICP-MS) uses a quadrupole mass spectrometer to separate the ions by their mass to charge ratios. In either case the final output is the calculated mass fractions of the elements in the sample. An advantage of ICP-MS is the ability to obtain isotopic information (since the ions are separated by mass). These methods reveal only the quantities and ratios of elements in the sample without any insight into the spatial distribution or crystallographic structure. Information regarding chemical compounds is also lost as the molecules are broken down by the high temperature plasma.

ICP-OES and ICP-MS cannot be used to detect Hydrogen, Carbon, Nitrogen or Oxygen within a sample. These elements are common constituents of sample solvents and are also present in the atmosphere. The ubiquity of these elements precludes their detection from being directly associated with the original sample. The halogens are difficult to detect as well, due to their high excitation energies [18].

The IAEA also suggests that Secondary Ion Mass Spectrometry (SIMS) and Thermal Ionization Mass Spectrometry (TIMS) be employed for isotopic and elemental analysis [19]. The use of SIMS in the analysis of trinitite has been reported in the literature [14]. For this current work a GBC Optimass 9000 ICP Time-of-Flight MS (ICP-TOF-MS) was used to obtain qualitative elemental and isotopic data for trinitite and synthetic nuclear melt glass. Careful calibration will allow for quantitative analysis in the future.

EDS analysis can also be used to determine the composition of the samples (as well as the spatial distribution of certain elements). For EDS analysis the INCA software by Oxford Instruments was employed in this study.

Powder X-ray Diffraction (P-XRD) analysis was performed on trinitite and synthetic melt glass using a Panalytical Empryean X-ray diffractometer with a Pixcel 3D detector. The x-ray source was a Cu anode set at 40 mA and 45 kV. A slit window of 1/4 degrees 2θ was used along with a 1/8 degrees 2θ anti-scatter diffraction grating. All samples were measured using a silicon (001) no-background sample holder and were set to spin at 4 revolutions/sec. All spectra were acquired from 10 degrees 2θ to 100 degrees 2θ. This data provides information on any crystalline phases within the samples. In the case of nuclear melt glass quartz is generally the only mineral present while the bulk of the sample matrix is highly amorphous.

The IAEA recommends the use of X-ray diffraction analysis (XRD), Gas Chromatography Mass Spectrometry (GC-MS) and Infrared analysis for obtaining information about the molecular constitution of a sample [19].

3.5.3 Radioactive Analysis

To characterize the fuel, fission products, activation products and decay products in nuclear debris requires thorough interrogation using gamma spectroscopy as well as alpha and beta radiography. For this study gamma-ray spectra were acquired using a Canberra Gamma Analyst High Purity Germanium (HPGe) detector equipped

with the GENIE 2K data processing software package. Alpha and beta radiography techinques have been used by others in the analysis of nuclear melt glass [5] [8] and similar analysis should be conducted on synthetic samples in the future.

Gamma Spectroscopy Examples of gamma spectra are shown in figures 3.1 and 3.2. Two trinitite samples were counted simultaneously for 4 days to generate the spectrum shown in figure 3.1. The trinitite spectrum shows characteristic peaks that are consistent with previously published data regarding radioactivity in trinitite [9].

The synthetic melt glass gamma-ray spectrum was also acquired over a 4-day count period. Figure 3.2 shows the synthetic melt glass spectrum prior to irradiation of the sample. This sample contained natural uranium. The fraction of uranium in the sample is consistent with a device containing 120 kilograms of natural uranium

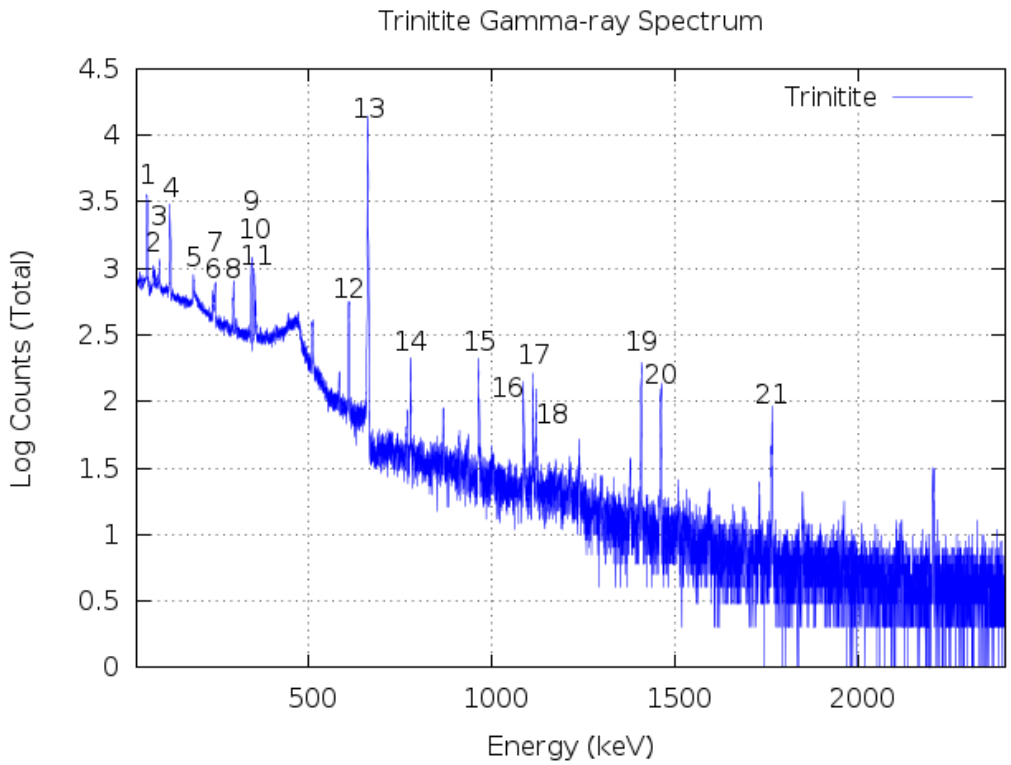

Figure 3.1: Trinitite Gamma Spectrum.

tamper and having a yield of 21 kilotons. These quantities are based on known information from the Trinity test [20].

The peaks labeled in figures 3.1 and 3.2 are explained in table 3.1. These peaks were identified using the GENIE 2K algorithm and the ID confidence value is reported in the final column of the table. Peaks very close in energy were given the same numerical label. Overlap between the trinitite and synthetic melt glass lines can be attributed to similar fractions of natural uranium (tamper). The synthetic sample does not contain fission or activation products.

Alpha Spectroscopy and Alpha Radiography Alpha spectroscopy will be useful for analyzing actinides such as plutonium and other alpha emitters which cannot be detected by gamma spectroscopy alone. Some actinides emit both alpha and gamma rays and thus the two analysis methods may be used in a complimentary

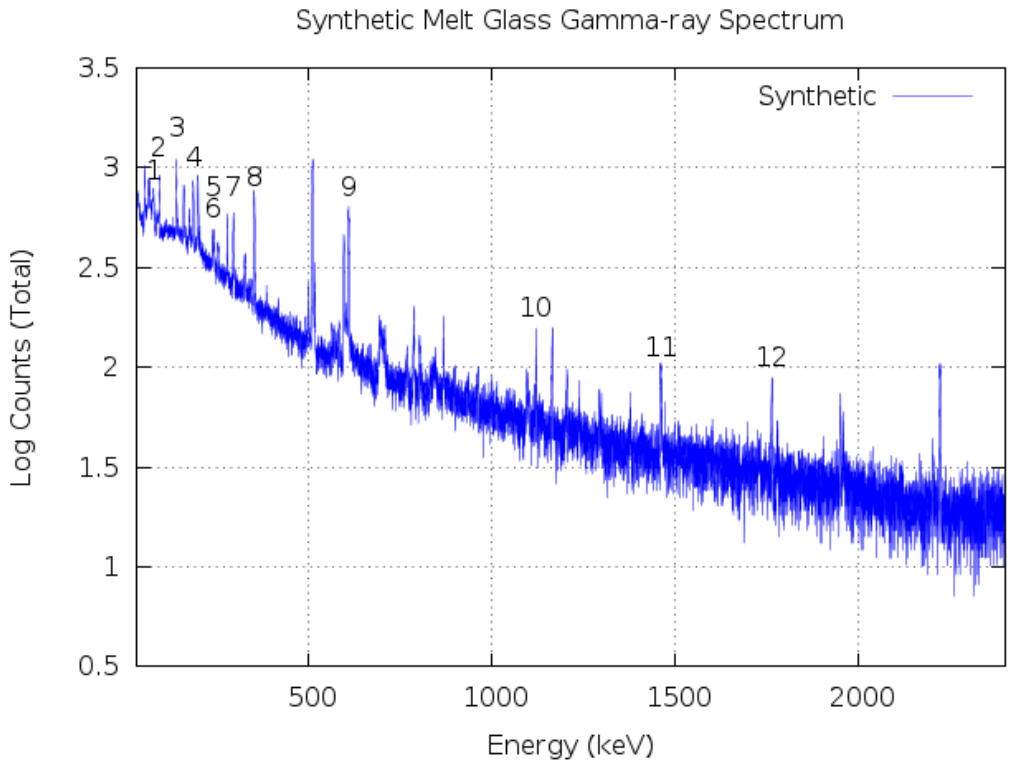

Figure 3.2: Synthetic Melt Glass Gamma Spectrum (prior to irradiation).

fashion to better characterize the radioactivity within the samples. With proper calibration the alpha and gamma activity may be quantified to determine specific concentrations and isotopic ratios. In addition, alpha radiography can be used to image alpha particle tracks and map the spatial distribution of alpha activity within the melt glass [5].

Beta Radiography Most fission products are beta emitters and can thus be analyzed using beta spectroscopy. However, most beta emitters are also gamma-ray emitters and gamma spectroscopy is often sufficient for detecting the presence of fission products. The spatial distribution of these fission products can only be discerned via beta radiography analysis. Alpha and beta radiography have been used together in the analysis of trinitite to show that alpha and beta activity is distributed differently within the melt glass [8].

Table 3.1: Explanation of gamma peaks labeled in figures 3.1 and 3.2. Trinitite (T) peaks are shown in the first column and synthetic (S) peaks in the second. For gamma lines found in both sample spectra the lower of the two confidence scores is reported. Activity (T/S) uncertainty is estimated to be 14 %. ^{232}Th was identified independently of the GENIE 2K nuclide ID algorithm.

Peak No.		GENIE 2K Reported Identifications					Suggested
T	S	E (keV)	ID	Conf.	$t_{1/2}$	Act. (Bq)	Source
1		59.54	^{241}Am	1.000	$4.33x10^{2}$ y	7.2	^{241}Pu Decay
2	1	77.11	^{212}Pb	0.551	$1.06x10^{1}$ h	0.9/0.4	^{232}Th Decay
2	1	77.11	^{214}Pb	0.727	$2.68x10^{1}$ m	3.2/1.8	^{238}U Decay
3	2	93.35	^{235}U	0.486	$7.04x10^{8}$ y	1.0/0.3	Tamper
3		93.35	^{228}Ac	0.603	6.13 h	7.6	^{232}Th Decay
4		121.78	^{152}Eu	0.958	$1.33x10^{1}$ y	6.4	Fission/Act.
	3	140.51	^{232}Th	UNK	$1.41x10^{10}$ y	UNK	Natural *
5	4	185.71	^{235}U	0.486	$7.04x10^{8}$ y	1.0/0.3	Tamper
5	4	186.21	^{226}Ra	0.966	$1.6x10^{3}$ y	4.3/4.3	^{238}U Decay
6	5	238.63	^{212}Pb	0.551	$1.06x10^{1}$ h	0.9/0.4	^{232}Th Decay
	6	241.98	^{214}Pb	0.727	$2.68x10^{1}$ m	3.2/1.8	^{238}U Decay
7		244.69	^{152}Eu	0.958	$1.33x10^{1}$ y	6.4	Fission/Act.
8	7	295.21	^{214}Pb	0.727	$2.68x10^{1}$ m	3.2/1.8	^{238}U Decay
9		344.27	^{152}Eu	0.958	$1.33x10^{1}$ y	6.4	Fission/Act.
10		351.1	^{211}Bi	0.476	2.14 m	11	^{235}U Decay
10	8	351.92	^{214}Pb	0.727	$2.68x10^{1}$ m	3.2/1.8	^{238}U Decay
11		356.01	^{133}Ba	0.486	$1.05x10^{1}$ y	0.8	Fission/Act.
12	9	609.31	^{214}Bi	0.541	$1.99x10^{1}$ m	13/2.2	^{238}U Decay
13		661.65	^{137}Cs	1.000	$3.00x10^{1}$ y	52	Fission
14		778.89	^{152}Eu	0.958	$1.33x10^{1}$ y	6.4	Fission/Act.
15		964.01	^{152}Eu	0.958	$1.33x10^{1}$ y	6.4	Fission/Act.
15		964.6	^{228}Ac	0.603	6.13 h	7.6	^{232}Th Decay
16		1085.78	^{152}Eu	0.958	$1.33x10^{1}$ y	6.4	Fission/Act.
17		1112.02	^{152}Eu	0.958	$1.33x10^{1}$ y	6.4	Fission/Act.
18	10	1120.29	^{214}Bi	0.541	$1.99x10^{1}$ m	13	^{238}U Decay
19		1407.95	^{152}Eu	0.958	$1.33x10^{1}$ y	6.4	Fission/Act.
19		1407.98	^{214}Bi	1.000	$1.99x10^{1}$ m	13	^{238}U Decay
20	11	1460.81	^{40}K	1.000	$1.28x10^{9}$ y	4.7/2.2	Natural
21	12	1764.49	^{214}Bi	0.514	$1.99x10^{1}$ m	13/2.2	^{238}U Decay

Chapter 4

Experimental Method for Producing Nuclear Melt-Glass Surrogates

Glass is produced by the high temperature melting of a matrix which contains three primary components: a glass former, a stabilizer and a flux. The most common glass former is SiO_2 which usually has a crystalline structure (e.g. quartz sand). Al_2O_3 is a common stabilizer which can share an oxygen atom with SiO_2 to form an amorphous matrix. Typical fluxes are alkaline metal oxides such as Na_2O, K_2O and CaO. These fluxes are strong bases and which will combine chemically with glass formers (e.g. SiO_2) and cause them to melt at lower temperatures. Conveniently, many soil types and minerals on the earth's surface contain the primary constituents described above. SiO_2 is ubiquitous and most soils also contained varying amounts of Al_2O_3, CaO, MgO, Fe_2O_3, K_2O, Na_2O and many other compounds which may combine to form glasses when subjected to temperatures in excess of 1200-1400 ^oC. In the case of nuclear debris (nuclear melt glass), the carrier material may contain concrete and other urban materials in addition to local soil. Because extensive nuclear testing has been conducted in desert environments, and desert soils are particularly

well suited for conversion to glass, the process described in this chapter will focus on production of a desert glass. The inclusion of urban materials and weapon components will be discussed as well. The sections that follow are intended to describe the process developed specifically for this project. More general information regarding glass making is available from numerous sources [21] [22] [23].

4.1 Equipment

Glass making can be accomplished with a relatively modest suite of equipment. A high temperature furnace is obviously essential, along with crucibles, tongs, and safety equipment. The choice of furnace was perhaps the most important step in developing the specific glass making process. This and other key pieces of equipment will be described in detail in the following subsections.

4.1.1 Furnace

For this process it was desirable to have a furnace with the highest possible operating temperature. SiO_2, the primary constituent of desert soils and most commercial glasses, has a melting temperature above 1600 ^oC which exceeds the peak temperature of most standard lab furnaces. Many silica glass forming matrices will melt at lower temperatures (1200-1400 ^oC) due to the presence of fluxes, however, the range of matrices and melting temperatures which may be encountered in this study was initially unknown and the ability to handle any potential scenario (or as many as possible) drove the decision to seek a furnace capable of heating up to 1800 ^oC.

The furnace used in this study is the Carbolite 18/4 High Temperature Furnace (HTF) rated at 1800 ^oC with a recommended working temperature range of 1400-1650 ^oC. This furnace has a small chamber with a height of 5.5 inches, a width of 5.5 inches and a depth of 7.5 inches. The chamber is heavily insulated and the elements are made of Molybdenum Disilicide. The unit is programmable and capable

of supporting rapid ramp rates and extended dwell times at elevated temperatures. More details regarding the employment of this furnace will be discussed in section 4.3.

4.1.2 Crucibles

The crucibles used must be made of materials with melting points well above the peak temperature of the specific melting process. Other considerations include volatility, durability, reactivity and cost. The composition of the melt matrix will influence the processing parameters and the appropriate crucible choice.

Zirconia (ZrO_2) has melting temperature well above the peak temperature of the furnace, and thus a zirconia crucible could safely be used for any process involving the Carbolite 18/4 HTF. The key disadvantage for zirconia is its tendency to crack under thermal stress. While the crucibles can withstand very high temperatures over extended time periods, any rapid temperature changes (rapid cooling in particular) will result in significant cracking of the material. There is also a risk of damaging the crucible during sample removal. Thus, zirconia crucibles are not ideal for processes that involve quenching or pouring of molten material. In this study it was found that many of the matrices used have an affinity for zirconia and tend to become fused inside the crucible during cooling.

Graphite will not melt at temperatures of interest in this study, however, it will oxidize readily above 500 ^oC and form carbon dioxide. In this study it was found that a crucible made of high purity graphite, with relatively thick walls, a mass of approximately 50 grams, and a capacity of 25.4 mL will become very brittle and will loose up to 80 percent of its mass after approximately 12 hours of processing time (including prolonged ramp-up and ramp-down periods at an average rate of 4.0 $^oC/min$). Thus, graphite crucibles are not suitable for processes that involve long dwell times at elevated temperatures and/or slow ramp rates. Another issue presented by graphite is the tendency for volatilized carbon to react with the sample

during melting. Post processing analysis has shown that a significant amount of carbon is incorporated into the final glass sample when using a graphite crucible.

Platinum has a lower melting temperature (approximately 1750 ^oC) and platinum crucibles have recommended working temperatures ranging from 1300 to 1550 ^oC, depending on the specific alloy used. Platinum crucibles are also very expensive, however, they will not volatilize or crack. One particular alloy, platinum with five percent gold (5AuPt), has a non-wetting property which promotes easier sample removal.

All of the crucibles described above have been tested for this project with mixed results. The graphite crucibles have proven effective at producing beads of glass which are easily removed. The negative aspect of graphite is its tendency to volatilize which limits the lifetime of the crucibles and also leads to the introduction of unwanted carbon into the glass sample. Samples melted in graphite crucibles were usually darker in color (compared to those melted in platinum) and were found to contain significant amounts of carbon (based on EDS analysis). The platinum crucibles do not crack or volatilize and can be used repeatedly for an indefinite period of time. However, Platinum reacts readily with silicon based material making sample removal very difficult. It has been observed that samples which contain more CaO (lime) will not fuse to the platinum and are easily removed post-processing. Unfortunately, trinitite and Nevada soil formulations contain less than 10 percent CaO and over 60 percent SiO2. Urban material, however, is expected to contain over 30 percent CaO and only about 40 percent SiO2. Platinum crucibles may be ideal for the melting of urban carrier material (or any matrix with a high CaO content).

4.1.3 Grinding and Mixing Equipment

A ceramic mortar and pestle is used to powder and thoroughly mix oxides prior to melting. An INDCO bench top roller mill with steel ball bearings (purchased from Sigma-Aldrich) is used to mix samples and produce a homogenized powder prior to

melting. This roller ball mill can also be used to polish larger rock or glass samples if necessary.

4.2 Temperature Requirements

The required melting temperature depends on the precise composition of the starting sample matrix. Complex phase diagrams must be consulted to determine the melting temperature of specific soils and mineral types. In some cases the melting temperature may be determined using sophisticated modeling techniques developed specifically for the glass making industry. More information regarding the calculation of glass liquidus temperatures is available at http://glassproperties.com/ [24].

4.3 Production Process

Extensive literature is available regarding the glass making process and analysis of various glass properties [25] [26] [27]. These resources are valuable, however, most processes are designed to produce glass with certain desirable qualities and a minimum number of defects. Some glasses are designed with specific optical properties for various industrial and technical applications. Others are desirable because of their stability (e.g. slow diffusion and leaching properties) and/or durability under various types of stress (e.g. elevated temperature and pressure).

Nuclear melt glass production is unique in that defects are often desirable as long as they are realistic. A key aspect of the debris production process is the rapid melting (shock melting) and rapid cooling (vitrification) of carrier materials (e.g. sand). The experimental procedures are designed to simulate the moment in time when the molten material inside the cloud re-solidifies and falls to the ground, cooling rapidly. The best way to accomplish this in a laboratory setting is to abruptly heat the sample to a temperature well above its usual melting point, hold the sample at

this temperature long enough to ensure nearly complete melting, and then quench the sample in sand or water at room temperature.

A question inevitably arises regarding the inability to experimentally recreate the intense heat and pressure associated with a true nuclear explosion. However, this may not be a significant concern as analysis of trinitite shows that quartz crystals are in their usual terrestrial form (alpha quartz) indicating that the temperature and over-pressure produced in the trinity test were not sufficient to create a higher pressure-temperature polymorph of quartz [11]. In this study it is assumed that any signatures from the blast and shock wave will be erased upon solidification and cooling of the material. The shock wave will impact the material while it is in a plasma state and thus should not alter the chemical structure or physical properties of the compounds which are ultimately formed (during the condensing and solidification phases). Solidification usually occurs 2-3 seconds after the explosion and the behavior of the material prior to that time remains largely a mystery.

4.4 Activation

Nuclear melt glass will contain fission products resulting from the chain reaction driving the explosion as well as activation products resulting from neutron induced transmutation of soil constituents, device components and various materials incorporated with the debris. These fission and activation products can be created artificially via neutron irradiation. This study takes advantage of the pneumatic tube system at the High Flux Isotope Reactor (HFIR) located at the Oak Ridge National Laboratory (ORNL). Pneumatic Tube 1 (PT-1) sustains a flux of $4x10^{14} ncm^{-2} s^{-1}$ with a thermal to resonance ratio of 35. The irradiation times can be determined based on the desired number of fissions. Because the quantity of nuclear melt glass is directly proportional to the yield of the weapon and the yield is directly proportional to the number of fissions it follows that the number of fissions per unit mass of debris should be essentially constant, assuming a uniform distribution. This oversimplified calculation

leads to a value of approximately $4x10^{14}$ fissions per gram of nuclear debris. In reality, this should represent an upper limit as the distribution is not uniform (the exact ratio will depend on location within the debris field and will range from 10^{12} to 10^{14} fissions per gram). The degree of non-uniformity will likely increase with distance from ground zero and since nuclear melt glass is found in the immediate vicinity of ground zero an average value should be sufficient for preliminary studies.

Using a thermal fission cross section of 577 barns for ^{235}U the fission rate for PT-1 is calculated to be $3.55x10^{10}$ fissions per μg (^{235}U) per minute of irradiation. Thus, the irradiation time will depend on the target number of fissions and the mass of ^{235}U used. For simplicity and ease of handling Uranyl Nitrate Hexahydrate (UNH) has been the primary form of nuclear fuel used in this study. UNH is appoximately 47 % uranium by weight and this uranium is assumed to be of natural enrichment (0.72 % ^{235}U). The required uranium concentration (within the debris) is calculated based on the quantity of fuel and tamper used and the yield of the device. The quantity of UNH incorporated into the synthetic samples is adjusted accordingly. The required irradiation times can easily be calculated based on the desired number of fissions and the calculated fission rate for ^{235}U in PT-1 at HFIR. Three examples are shown in table 4.1.

Table 4.1: UNH mass and corresponding ^{235}U mass per gram of nuclear melt glass for three notional devices. Irradiation times are based on a 1-gram melt glass sample irradiated in PT-1 at HFIR to produce 10^{12} fissions.

Notional Device	UNH mass (g)	^{235}U mass (g)	Irr. Time (m)	ϕ (n/cm^2)
Gadget Mod1	$3.70x10^{-5}$	$1.26x10^{-7}$	218	$5.22x10^{18}$
Gadget Mod2	$7.09x10^{-4}$	$2.42x10^{-6}$	11.4	$2.73x10^{17}$
IND1	$1.95x10^{-3}$	$6.66x10^{-6}$	4.13	$9.91x10^{16}$

The Gadget Mod1 device is meant to simulate the Gadget device used in the Trinity test, but without the plutonium fuel. It has been suggested that approximately 30 % of the energy generated by the Trinity explosion resulted from the fission of uranium in the tamper [28]. The modest number of fissions generated

(by 3 hours and 38 minutes of neutron irradiation) in the Gadget Mod1 debris could represent the fraction from the tamper. This could provide a useful comparison to future debris surrogates which will include the plutonium fuel. The Gadget Mod2 device is a notional, low-yield (1 kT) version of the Gadget device. IND1 is intended to represent a notional improvise nuclear device with a crude design and a 1 kT yield. The carrier material for all of these samples are similar (see chapter 5). Only the fuel and tamper fractions are varied.

Chapter 5

Debris Formulations

5.1 Composition

The composition of surface debris near ground zero depends on two primary factors: the type of device employed and the composition of the local environment. Contributions from these two key components will be considered here.

5.1.1 Device

Some device components should not and will not be discussed here. However, the type of fuel required to build a working nuclear device is common knowledge and produces important signatures within the nuclear debris. For simplicity, the device will be treated as a spherical core of either uranium or plutonium fuel contained within a spherical blanket of tamper. The tamper may be made of uranium, tungsten, lead or gold. The International Atomic Energy Agency (IAEA) has published official "significant quantities" of enriched uranium and plutonium. These quantities will be used here. It is estimated that 25 kilograms of weapons grade uranium, or 8 kilograms of weapons grade plutonium would be required to build a functioning nuclear bomb [29]. Based on these masses and the known densities of uranium and plutonium, the dimensions of a spherical core of either fuel can be easily calculated. The tamper is

assumed to be 17 cm thick, based on calculations published in the Los Alamos Primer [30]. The number of fissions required to produce a given yield is also easily calculated, and from this the amount of fissioned fuel can be determined. Estimates have been published by Glasstone and others regarding the quantity of debris produced per kiloton of yield. The trinity test employed a 20 kiloton device and it is estimated that 7500 metric tons of debris were produced. Assuming a linear relationship, this would imply that approximately 375 metric tons of melt glass are produced per kiloton of yield [8]. For a contained subsurface burst the quantity of melt glass may be higher - up to 700 metric tons per kiloton [4]. The DELFIC Model predicts a quantity of debris incorporated into the rising fireball (following a surface burst) based on conservation of momentum, mass, heat, and turbulent kinetic energy. This model implies a relationship that is not perfectly linear but gives a quantity of about 800 metric tons for a 1 kiloton device [31]. In any case, an estimate can be obtained that is fairly reliable, and thus, knowing the type of device and the yield, the fraction of residual fuel found in the debris can be estimated. In addition, the fission product and tamper fractions can be calculated. The fission products, un-fissioned fuel and tamper will make up a very small fraction of a given debris sample. The bulk of the debris will be comprised of carrier material.

5.1.2 Local Environment

The carrier material will be characteristic of the local environment. In the case of trinitite, the composition is predominately sand, clay and feldspar. In an urban environment concrete, steel and glass would be prevalent as well.

5.2 Simple Formulations

Oxide mixtures were prepared in accordance with published data regarding trinitite composition [11]. The Standard Trinitite Formulation (STF) for green trinitite is

Table 5.1: Comparison of published trinitite data [11] and the synthetic trinitite formulation (STF). Both elemental and compound data are shown.

Weight Percent by Compound			Weight Percent by Element		
Compound	Trinitite	Synthetic	Element	Trinitite	Synthetic
SiO_2	$6.42x10^{-1}$	$6.42x10^{-1}$	Si	$3.00x10^{-1}$	$3.00x10^{-1}$
Al_2O_3	$1.43x10^{-1}$	$1.43x10^{-1}$	Al	$7.55x10^{-2}$	$7.55x10^{-2}$
CaO	$9.64x10^{-2}$	$9.64x10^{-2}$	Ca	$6.88x10^{-2}$	$6.88x10^{-2}$
FeO	$1.97x10^{-2}$	$1.97x10^{-2}$	Fe	$1.53x10^{-2}$	$1.53x10^{-2}$
MgO	$1.15x10^{-2}$	$1.15x10^{-2}$	Mg	$6.90x10^{-3}$	$6.90x10^{-3}$
Na_2O	$1.25x10^{-2}$	$1.25x10^{-2}$	Na	$9.24x10^{-3}$	$9.24x10^{-3}$
K_2O	$5.13x10^{-2}$	n/a	K	$4.26x10^{-2}$	$4.26x10^{-2}$
KOH	n/a	$6.12x10^{-2}$	H	n/a	$1.10x10^{-3}$
MnO	$5.05x10^{-3}$	$5.05x10^{-3}$	Mn	$3.93x10^{-4}$	$3.93x10^{-4}$
TiO_2	$4.27x10^{-3}$	$4.27x10^{-3}$	Ti	$2.58x10^{-3}$	$2.58x10^{-3}$
U	$1.60x10^{-5}$	n/a	U	$1.60x10^{-5}$	$1.60x10^{-5}$
UNH	n/a	$3.37x10^{-5}$	N	n/a	$1.88x10^{-6}$
O_2	n/a	n/a	O	$4.60x10^{-1}$	$4.69x10^{-1}$
Total	$9.81x10^{-1}$	$9.91x10^{-1}$	Total	$9.81x10^{-1}$	$9.91x10^{-1}$

shown in figure 5.1 where concentrations are reported as weight fractions. Potassium hydroxide (KOH) is used in place of potassium oxide (K2O) due to the limited availability and high reactivity of this oxide. The KOH compound weight percent is adjusted to obtain the correct potassium concentration.

The STF is used as a starting point for the development of synthetic nuclear melt glass specifications. Individual oxide powders are carefully weighed and then thoroughly mixed using a mortar and pestle. KOH pellets and Na2O beads were powdered prior to fine mixing. The uranium weight fraction is based on a tamper mass of 120 kg [20] used in the gadget device, and an estimate of 7500 metric tons of melt glass produced by the Trinity test [8]. For initial studies it is assumed that the total mass of tamper material (natural uranium) is dispersed and distributed uniformly within the nuclear melt glass. For notional improvised nuclear devices the fuel quantities are based on IAEA significant quantities and tamper quantities are based on early crude estimates, as discussed in the previous section.

UNH is used in the laboratory in appropriate quantities to achieve the correct fraction of uranium (UNH is 47.41 percent uranium by weight). The oxide concentrations listed in figure 5.1 are based on chemical analysis of glassy regions within a trinitite fragment as well as several trinitite beads [11]. The STF composition is based on an average of these published data points. The UNH concentration and the corresponding uranium, nitrogen and hydrogen concentrations are based on calculation.

UNH decomposes at 200-350 degrees celsius to form UO_3 (with a monohydrate intermediate). Complete conversion to UO_3 occurs in approximately 2 minutes at temperatures above 350 degrees celsius [32]. It is possible that oxygen, nitrogen dioxide, and water molecules from the UNH and from the atmosphere, along with carbon from the graphite crucibles (and the atmosphere), will react with other metals in the sample (during melting and subsequent cooling) to produce various oxide compounds. These products are not entirely undesirable from an experimental standpoint as the atmosphere surrounding a nuclear explosion will contain gases and volatilized organic matter.

The majority of the samples discussed in the results section of this thesis do not contain uranium. The tamper was omitted to avoid potential challenges associated with handling of radioactive samples and because small quantities of uranium (or UNH) will not impact the final morphology of the samples (which is the primary concern of this present study). Uranium has been incorporated into several samples which will eventually be activated via neutron irradiation, then analyzed and reported shortly. The gamma-ray spectrum from one sample containing uranium is shown in chapter 3.

It should also be noted that the STF does not include additional refractory elements as suggested in chapter 2 (for the purpose of weighting the fission curve to simulate refractory debris from a fission device). This method will be explored in future studies after unfractionated debris surrogates are fully characterized.

The specific samples discussed in chapter 4 (table 4.1) are based on the known design of the Gadget device used in the Trinity test (Gadget Mod1 and Mod2) or the crude estimations described in this chapter (IND1). Future samples, based on purely notional events, will be produced in a manner similar to IND1.

Chapter 6

Results

6.1 Surface Morphology

By visual inspection of trinitite and synthetic melt glass many macroscopic similarities are immediately apparent (figures 6.1 and 6.2). The physical appearance of the surrogate debris is very similar to trinitite with a heterogeneous and vesicular appearance observable at the macroscopic level. The trinitite samples are greenish brown in color and contain numerous vesicles some rather large. The synthetic melt glass also has a greenish tint although the shade is somewhat lighter and the darker regions appear more gray than brown. Color variations are obvious in all of the samples shown here as well as those observed at the lab (both trinitite and synthetic melt glass). Both real and synthetic debris samples can also be described as having a blotchy appearance with some textural variations. Perhaps the most noteworthy similarity (based purely on visual inspection) is the vesicular appearance of both real and synthetic debris samples.

SEM imaging showed similar surface features at the 10 micron level. Figure 6.3 provides two SEM BSE micrographs of the same trinitite sample showing detailed surface morphology containing numerous cracks, pores and particle inclusions along with a varied surface texture. In addition, there is evidence of compositional

heterogeneity on the surface, consistent with previously published SEM analysis of trinitite [14]. The lighter colored areas likely correspond to regions with high titanium, iron or calcium content. The darker regions probably contain a higher percentage of silicon, aluminum or magnesium.

Figure 6.1: Photos of Trinitite (top) and Synthetic (bottom) Nuclear Melt Glass.

The trinitite sample (figure 6.3) contains numerous vesicles and cracks as well as evidence of surface flows. Both images reveal features which indicate that random

Figure 6.2: Photos of Trinitite (top) and Synthetic (bottom) Nuclear Melt Glass.

mixing and flows occurred during the rapid cooling process. These features are also consistent with early documented observations of trinitite [10].

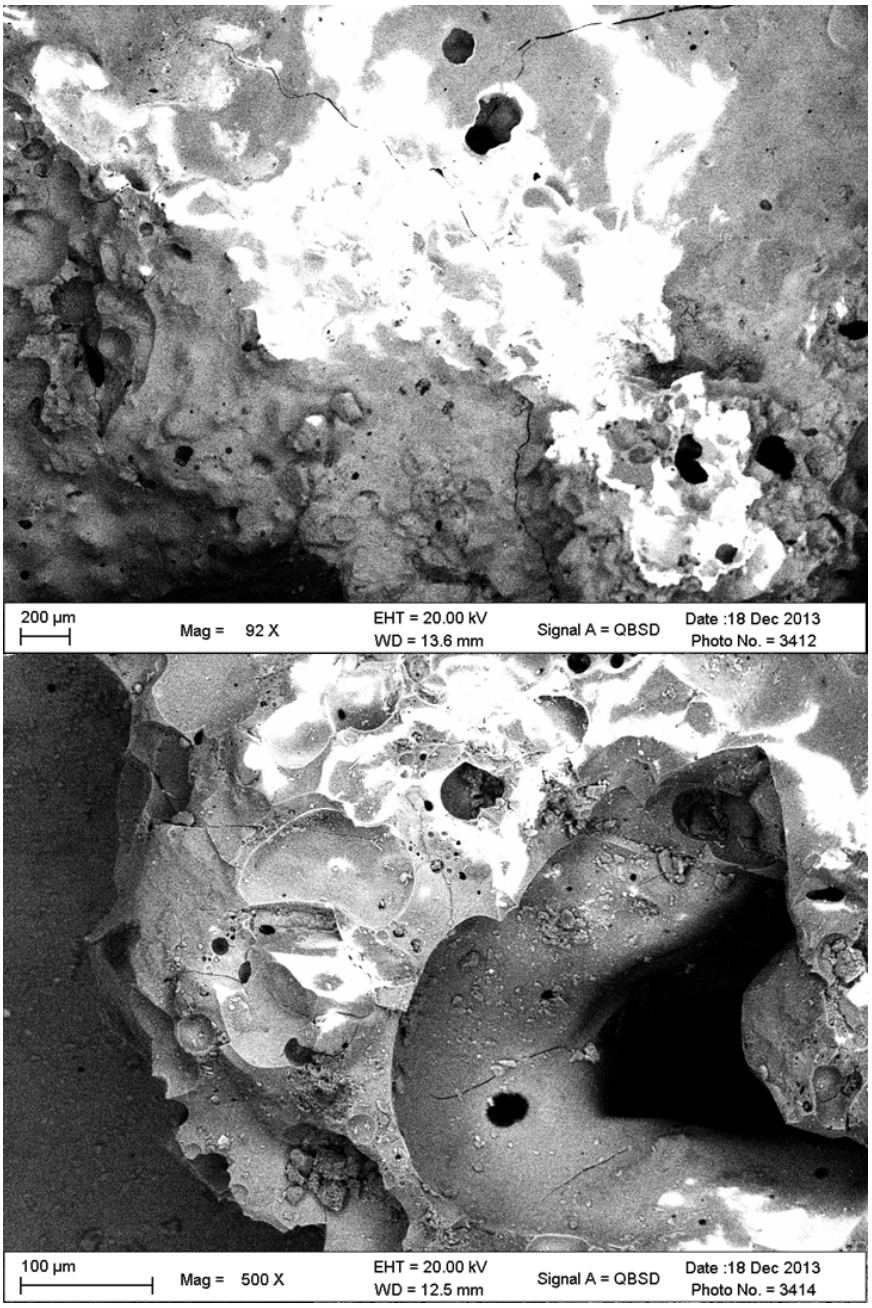

Figure 6.3: SEM BSE micrographs showing two different regions of the same trinitite sample; Top: 92 times magnification; Bottom: 500 times magnification.

Figure 6.4 compares two synthetic melt glass samples produced from the same Nevada soil matrix, but with different processing parameters. The top image in figure 6.4 shows the surface of a sample which was heated between 1385 and 1459 degrees Celsius for 12.5 minutes. The lower image in the same figure shows the surface of a sample (with identical composition) which was heated for 60 minutes at 1500 degrees Celsius. The longer melt at higher temperature produces a glassy surface which is more uniform. The image of the 12.5 minute melt reveals a distinct textural change. A glassy vesicular matrix is seen on the right while a grainy matrix is seen on the left. Elemental mapping via energy dispersive spectroscopy (EDS) suggests the grainy region has a higher iron concentration.

Figure 6.5 compares two synthetic nuclear melt glass fragments to a trinitite fragment of similar size. The images on the left were taken at 500 times magnification while the images on the right were taken at 200 times magnification. The top images show the features of the trinitite fragment and the bottom images show the two synthetic fragments. The synthetic sample imaged in the lower left quadrant was produced by melting 2 grams of STF powder at 1400 degrees Celsius for 60 minutes. The sample imaged in the lower right quadrant was produce by melting 2 grams of STF powder at 1500 degrees Celsius for 45 minutes. Both synthetic samples were melted in a graphite crucible.

Both synthetic samples were similar in color and physical appearance. The key features revealed in the figure 6.5 images are the vesicular nature and varied texture of both trinitite and synthetic nuclear melt glass. Similar features have also been observed in nuclear melt glass from underground testing [5] [4].

6.2 Chemical Composition and Crystallinity

EDS analysis was performed to estimate the elemental content of one trinitite sample and two synthetic melt glass samples. One synthetic samples was produced using the STF while the other was based on a Nevada soil matrix. The elemental data for

these samples is consolidated in table 6.1. In the case of synthetic trinitite, direct comparison of data in table 6.1 and table 5.1 indicates that elemental composition on the surface may not be representative of the entire sample. Because melting occurs in

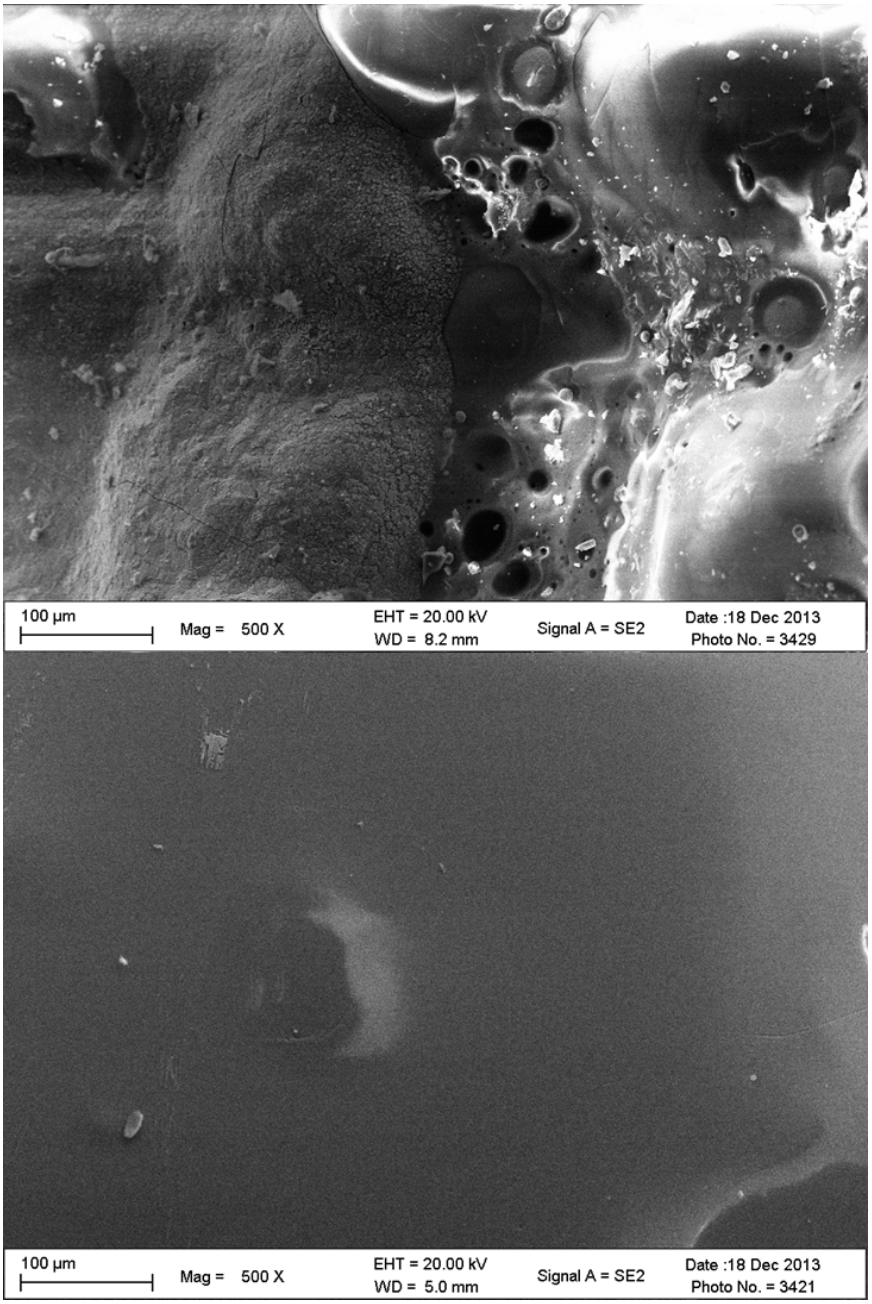

Figure 6.4: SEM images of two samples with the same composition but different processing parameters. The bottom image shows the surface of a sample which was melted approximately five times longer at a higher temperature.

open air the chemistry of the sample may change due to high temperature reactions with oxygen and nitrogen (in the atmosphere) as well as carbon (from the crucible and the atmosphere). Compounds with the highest oxygen content may be concentrated near the surface of the sample. Preliminary EDS mapping reveals a non-uniform elemental distribution in both trinitite and synthetic melt glass fragments. Data in table 6.1 is thus only semi-quantitative and is shown primarily to demonstrate the consistency between trinitite and synthetic melt glass when the same analysis techniques are applied to both.

The starting formulation for the Nevada matrix contains a higher fraction of SiO^2 and $Al2O^3$ with a relatively low CaO content (compared to the STF). Nuclear melt glass from the Nevada National Security Site is not available to UT for comparison. The synthetic Nevada melt glass samples are included here to show that different debris matrices can be produced to model a variety of scenarios. The Nevada

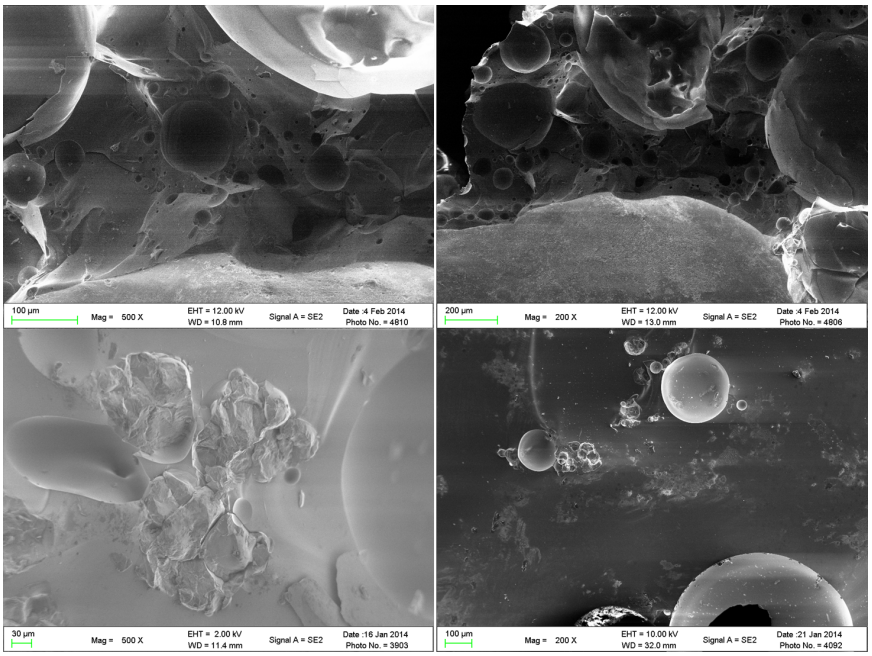

Figure 6.5: SE images comparing trinitite and synthetic melt glass samples. The top images show the morphology of a particular trinitite fragment while the bottom images show two separate synthetic samples.

Table 6.1: Elemental composition data (based on EDS analysis) for trinitite and two synthetic melt glasses (one made from the STF and one from a simulated Nevada soil mixture).

	Approximate Weight Fractions		
Element	Trinitite	STF Glass	Nevada Glass
Si	$2.18x10^{-1}$	$2.21x10^{-1}$	$2.22x10^{-1}$
Al	$4.63x10^{-2}$	$5.54x10^{-2}$	$1.14x10^{-2}$
Ca	$3.70x10^{-2}$	$3.03x10^{-2}$	$1.42x10^{-2}$
K	$1.46x10^{-2}$	n.d.	n.d
Na	n.d.	$1.74x10^{-2}$	$2.88x10^{-2}$
Fe	n.d.	$8.00x10^{-3}$	$1.34x10^{-2}$
Mg	n.d.	n.d	$1.50x10^{-2}$
O	$6.85x10^{-1}$	$6.68x10^{-1}$	$5.93x10^{-1}$

formulation may be further analyzed and optimized in the future, along with a formulation for urban debris.

P-XRD analysis was performed to investigate the morphology and chemistry of both trinitite and synthetic nuclear melt glass samples. The trinitite proved to be largely amorphous with the exception of a few peaks which are predominantly matched with quartz. Patterns were matched using the search and match function within the Panalytical analysis software. The synthetic samples also contain quartz. The number and intensity of the observed peaks appears to depend rather sensitively on the melt time and temperature.

The two images shown in figure 6.6 are of the same feature on a fragment of synthetic melt glass. The SE image shows only topographical features while the BSE image also shows relative differences in atomic number. The dark spots in the BSE image are low-Z grain inclusions within the glassy matrix. Point EDS reveals that several of these inclusions are carbon debris particles picked up from the graphite crucible in which the sample was melted. At least one grain proved to be predominantly silicon (presumably a partially melted quartz inclusion). Similar inclusions have been found in trinitite samples [11] [16]. Partially melted or un-melted

quartz grains are undoubtedly the source of the crystalline peaks which appear in the P-XRD data of both trinitite and synthetic melt glass samples.

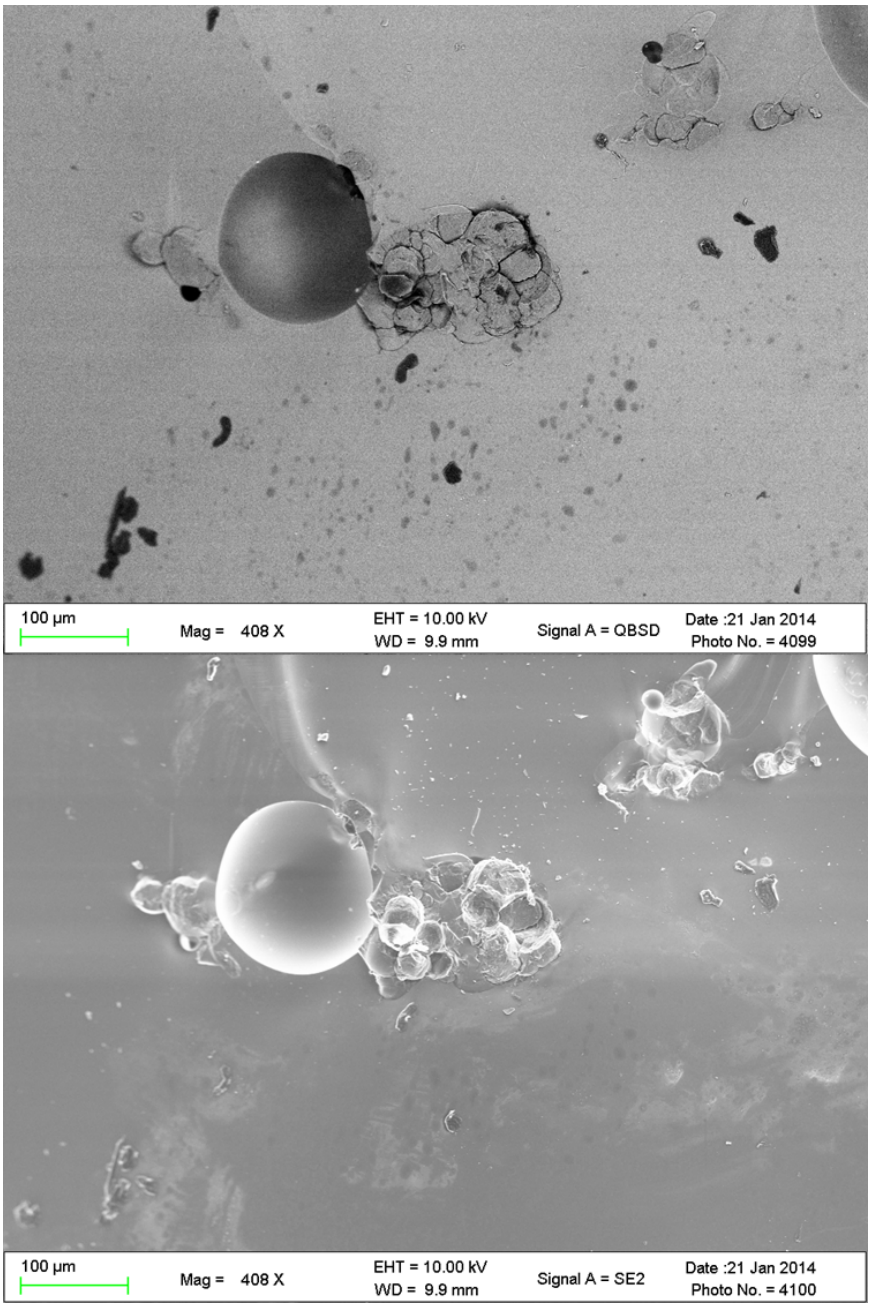

Figure 6.6: BSE (top) and SE (bottom) images of the same area on the surface of a fragmented synthetic melt glass sample.

The sample imaged in figure 6.6 was produced using the STF and melted for 45 minutes at a temperature of 1500 degrees Celsius. The P-XRD pattern for this sample is shown in figure 6.9 and compared to a similar sample with a lower processing temperature.

In an effort to quantify the amorphous character of a sample the individual P-XRD peaks may be analyzed and compared to the background. By summing the counts under the prominent peaks and dividing by the total number of counts an approximate percentage can be assigned to the crystallinity of the sample. This analysis was performed on the patterns shown in figures 6.7 and 6.8 since they represent the best correlation between a real and synthetic melt glass sample.

By the above method it is estimated that the trinitite is 5.7 percent crystalline and 94.3 percent amorphous while the synthetic melt glass is 6.8 percent crystalline and 93.2 percent amorphous. The particular synthetic sample analyzed here was melted at 1400 degrees Celsius for 45 minutes. This sample is compared to another synthetic

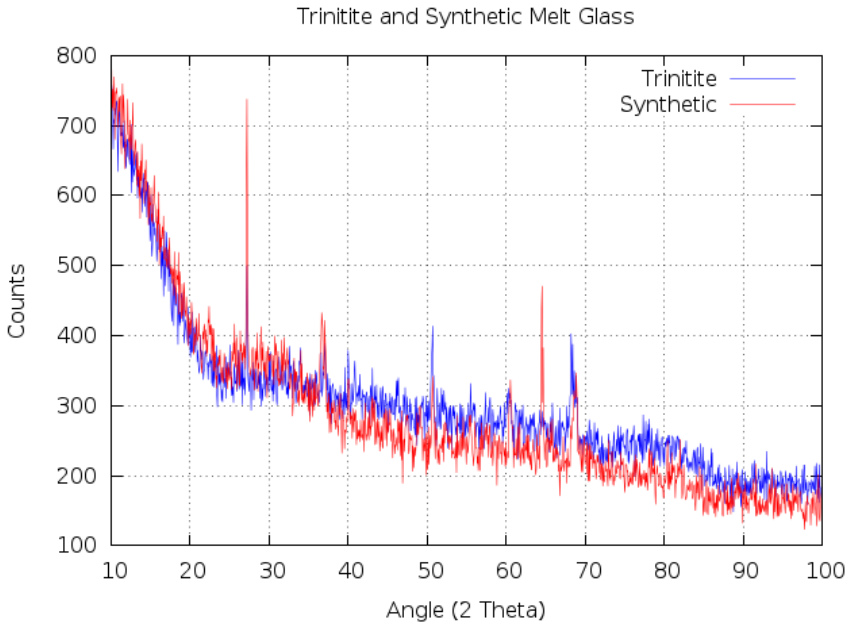

Figure 6.7: Trinitite P-XRD pattern (blue) compared to a Synthetic Melt Glass P-XRD pattern (red).

sample in figure 6.10, where it can be seen that a processing temperature of 1500 degrees Celsius produces a sample that is almost completely amorphous.

An interesting feature is observed in figure 6.9 which shows the P-XRD pattern of a particular synthetic melt glass sample. The non-quartz peak in the pattern (at approximately 22 degrees 2θ) is a strong match for cristobalite which is a high temperature polymorph of silica. Cristobalite is thermodynamically stable at or above 1470 degrees Celsius and will gradually revert back to quartz at lower temperatures. However, it has been observed to survive for long periods at lower temperatures in meteorites and lunar rocks. It has been suggested that rapid cooling of molten rock is conducive to the formation of cristobalite [33]. The synthetic melt glass analyzed here was heated at 1500 degrees Celsius for 15 minutes and then quenched in sand at room temperature. This particular sample was produced using a simplified matrix which did not include several of the minor constituents in the STF (TiO_2, MnO, and KOH) and included Na_2SO_4 in place of Na_2O. SEM BSE images of the surface of this sample are shown in figure 6.5.

6.3 Effect of Melting Temperature on Morphology and Crystallinity

It is well documented that quartz is generally the only mineral that survives in trinitite [11] [20]. It is desirable that surrogate melt glass exhibit a similar degree of crystallinity. The processing parameters which have the greatest impact on the amorphous or crystalline nature of the melt glass are temperature, melt time and cooling rate. Figure 6.10 compares two synthetic samples with the same composition and identical processing parameters, with the exception of the melting temperature. Both samples were melted for 45 minutes in graphite crucibles. A 100 degree increase in melting temperature significantly reduces the number and intensity of crystalline peaks identified via P-XRD analysis.

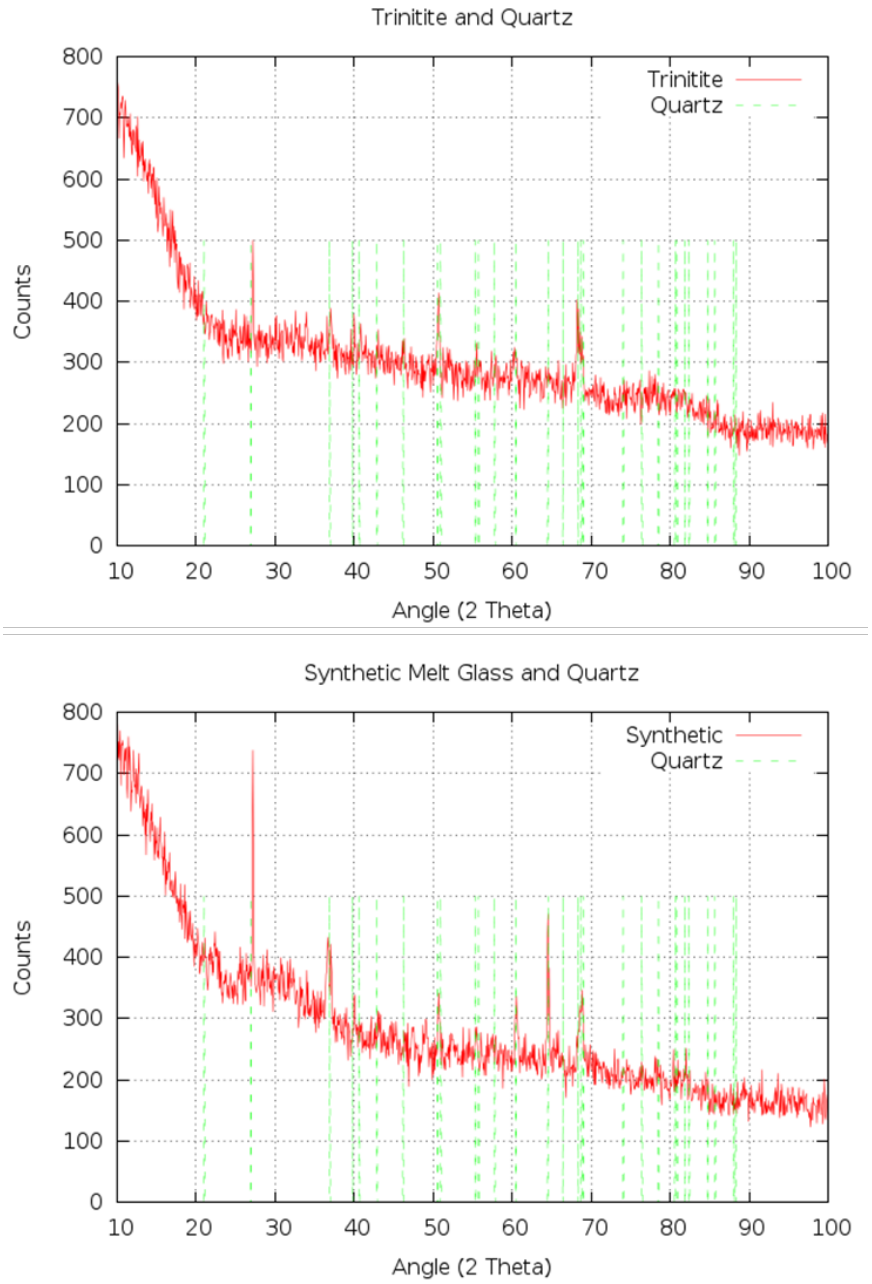

Figure 6.8: Top: A Trinitite sample P-XRD pattern; Bottom: A Synthetic Melt Glass P-XRD pattern; Dashed green lines show the location (not the intensity) of quartz peaks for comparison in each plot. Observed peaks show good agreement with the quartz assignment.

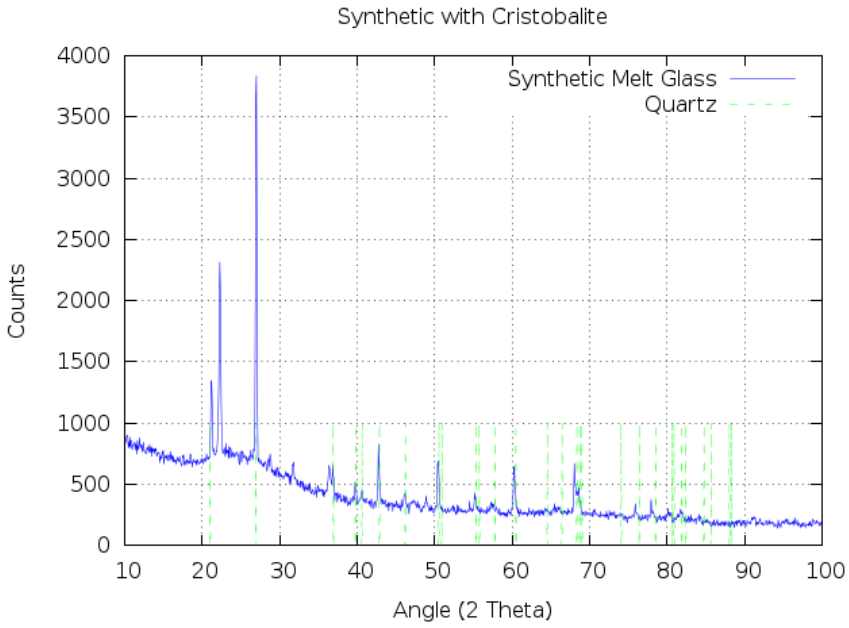

Figure 6.9: Synthetic Trinitite P-XRD pattern with quartz peaks identified (green dashed lines). The prominent non-quartz peak has been matched with cristobalite.

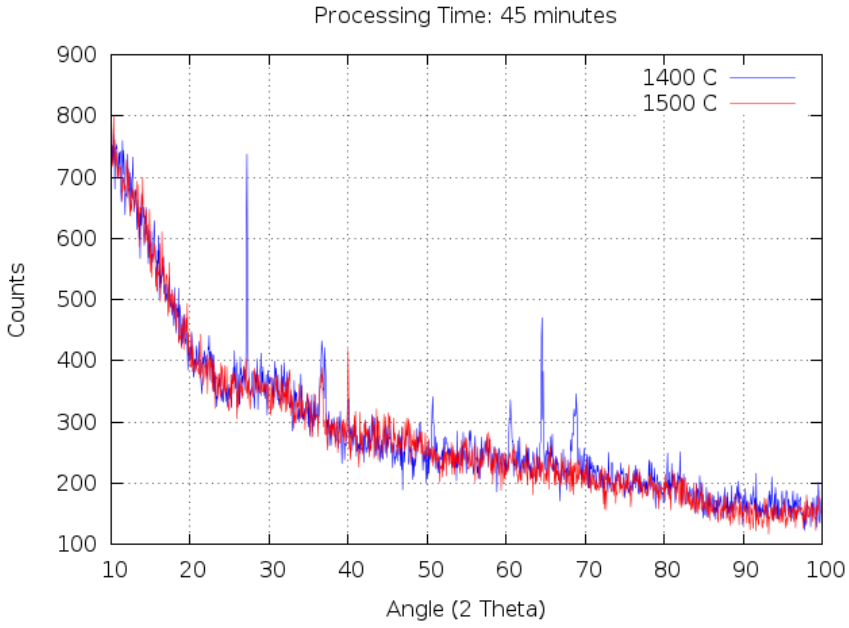

Figure 6.10: P-XRD Crystalline peak comparison of two synthetic samples melted at different temperatures (blue: 1400 C, red: 1500 C).

6.4 Effect of Melting Time on Morphology and Crystallinity

Figure 6.11 compares two surrogates with the same composition, which were both melted at 1400 degrees Celsius, but for different durations. The x-ray spectra are very similar with the exception of a prominent peak at 65 degrees 2θ which is seen only in the 45 minute melt data. This peak is easily associated with quartz, as are the remainder of the peaks seen in both spectra. The longer melt retains some quartz but with fewer prominent peaks. This comparison demonstrates that a 25 percent increase in melting time produces a noticeable decrease in crystallinity.

Referring back to figure 6.4, the effect of melting time on surface morphology is also apparent. The samples shown in figure 6.4 were also analyzed using P-XRD and it was found (not surprisingly) that the sample with the longer melt time was

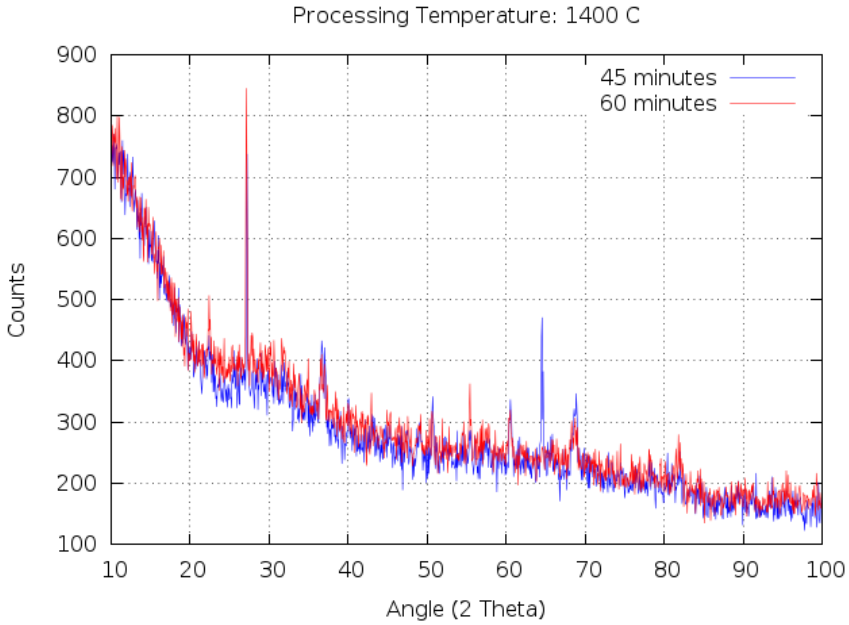

Figure 6.11: P-XRD Crystalline peak comparison of two synthetic samples with different melt times (blue: 45 min, red: 60 min).

highly amorphous compared to the companion sample with the shorter melt time and somewhat erratic processing temperature (starting at 1459 C and ending at 1385 C).

Chapter 7

Conclusions and Future Work

A method for producing synthetic nuclear melt glass has been tested and the samples characterized using P-XRD, SEM, EDS and gamma spectroscopy. The starting formulation for the synthetic samples was based on published data partially quantifying the oxide composition of trinitite (the original and most readily available form of nuclear melt glass). It has been shown that a reasonable set of processing parameters can be employed to produce synthetic melt glass with chemical and morphological properties very similar to trinitite. In particular, a high degree of vitrification can be achieved at temperatures between 1400 and 1500 degrees celsius with melt times between 30 and 60 minutes.

Additional analysis will be required to optimize the production process. It is clear that, from a chemical and morphological standpoint, a realistic surrogate is obtainable. Optical, morphological and chemical data collected on trinitite and synthetic melt class proved to be comparable.

Modeling tools are available for predicting the types and quantities of fission products, activation products, and actinides contained in a notional sample. These tools, as described in chapter 2, can also be employed to conduct neutronics calculations. Based on such calculations, a method has been suggested which would

allow for the adjustment of fission and activation product signatures by careful manipulation of the initial sample chemistry.

The scheme for production and activation of nuclear melt glass samples is outlined in chapter 4. The analysis of activated samples will be an important next step for this program. The irradiation parameters suggested are tailored for activation at HFIR, however, other activations routes are available and may be considered in the future.

Future work will also include the preparation of urban debris samples with varying quantities of soil, concrete, metals and window glass. Preliminary work suggests that small changes in debris composition will lead to different processing requirements. The melting temperature is a strong function of chemical composition and the choice of crucible (e.g. platinum or graphite) may also depend on the sample composition.

In addition to the production of bulk surface debris, which is the focus of this thesis, particulate debris production routes will also be explored through the collaborative efforts of UT and ORNL. A plasma system connected to a particle dispersion chamber has been proposed as a mechanism for the production of nuclear fallout particles. Knowledge gained from the production of nuclear melt glass and fallout particles, in conjunction with fallout modeling predictions used for validation, will lead to the development of more effective forensic analysis techniques.

Bibliography

[1] Congress, "Public Law 111 140, 111th Congress, Nuclear Forensics and Attribution Act," pp. 1–6, 2010. 1, 2

[2] A. Klingensmith, "National Center for Nuclear Security, The Nuclear Forensics Project," NCNS, Tech. Rep., 2012. 2

[3] Samuel Glasstone and P. Dolan, *Effects of Nuclear Weapons*, 3rd ed. United States DOD/DOE, 1977. 4, 5

[4] A. B. Kersting and D. K. Smith, *Observations of Nuclear Explosive Melt Glass Textures and Surface Areas*. Lawrence Livermore National Laboratory, 2006. 5, 6, 23, 24, 26, 27, 45, 53

[5] G. F. Eaton and D. K. Smith, "Aged nuclear explosive melt glass : Radiography and scanning electron microscope analyses documenting radionuclide distribution and glass alteration," *Journal of Radioanalytical and Nuclear Chemistry*, vol. 248, no. 3, pp. 543–547, 2001. 5, 24, 26, 32, 34, 53

[6] D. K. Smith and W. L. Bourcier, "The Production and Dissolution of Nuclear Explosive Melt Glasses at Underground Test Sites in the Pacific Region," International Atomic Energy Agency, Monte Carlo, Principality of Monaco, Tech. Rep., 1998. 5, 25, 26, 28

[7] C. W. Olsen, "Time History of the Cavaity Pressure and Temperature Following a Nuclear Detonation in Alluvium," *Journal of Geophysical Research*, vol. 72, no. 20, 1967. 6

[8] F. Belloni, J. Himbert, O. Marzocchi, and V. Romanello, "Investigating incorporation and distribution of radionuclides in trinitite." *Journal of environmental radioactivity*, vol. 102, no. 9, pp. 852–62, Sep. 2011. [Online]. Available: http://www.ncbi.nlm.nih.gov/pubmed/21636184 7, 23, 27, 32, 34, 45, 46

[9] P. P. Parekh, T. M. Semkow, M. a. Torres, D. K. Haines, J. M. Cooper, P. M. Rosenberg, and M. E. Kitto, "Radioactivity in trinitite six decades later." *Journal of environmental radioactivity*, vol. 85, no. 1, pp. 103–20, Jan. 2006. [Online]. Available: http://www.ncbi.nlm.nih.gov/pubmed/16102878 7, 32

[10] C. S. Ross, *Optical Properties of Glass from Alamogordo , New Mexico*, 1948. 7, 52

[11] N. Eby, R. Hermes, N. Charnley, and J. a. Smoliga, "Trinitite-the atomic rock," *Geology Today*, vol. 26, no. 5, pp. 180–185, Sep. 2010. [Online]. Available: http://doi.wiley.com/10.1111/j.1365-2451.2010.00767.x x, xi, 7, 9, 10, 25, 26, 41, 45, 46, 47, 56, 59

[12] S. Goluoglu, N. Landers, L. Petrie, and D. Hollenbach, "Scale : A Comprehensive Modeling and Simulation Suite for Nuclear Safety Analysis and Design (ORNL/TM-2005/39)," 2011. 10

[13] V. J. Jodoin, R. W. Lee, D. E. Peplow, and J. P. Lefebvre, "Application of the ORIGEN Fallout Analysis Tool and the DELFIC Falloout planning Tool to National Technical Nuclear Forensics," *ANS EPRRSD - 13th Robotics & Remote Systems for Hazardous Environments - 11th Emergency Preparedness & Response*, 2011. 10, 11, 19

[14] J. Fahey, C. J. Zeissler, D. E. Newbury, J. Davis, and R. M. Lindstrom, "Postdetonation nuclear debris for attribution." *Proceedings of the National Academy of Sciences of the United States of America*, vol. 107, no. 47, pp. 20 207–12, Nov. 2010. [Online]. Available: http://www.pubmedcentral.nih.gov/articlerender.fcgi?artid=2996690&tool=pmcentrez&rendertype=abstract 27, 29, 31, 50

[15] E. C. Freiling and M. A. Kay, "Radionuclide Fractionation in Air-Burst Debris," U.S. Naval Radiological Defense Laboratory, San Francisco, CA, Tech. Rep. September, 1965. 28

[16] J. J. Bellucci and A. Simonetti, "Nuclear forensics: searching for nuclear device debris in trinitite-hosted inclusions," *Journal of Radioanalytical and Nuclear Chemistry*, vol. 293, no. 1, pp. 313–319, Feb. 2012. [Online]. Available: http://link.springer.com/10.1007/s10967-012-1654-9 29, 56

[17] J. B. Bindell, "Scanning Electron Microscopy," pp. 70–84, 1992. 29, 30

[18] X. Hou and B. T. Jones, "Inductively Coupled Plasma / Optical Emission Spectrometry," pp. 9468–9485, 2000. 30

[19] IAEA, "Nuclear Forensics Support," IAEA, Vienna, Austria, Tech. Rep. 2, 2006. 31

[20] C. Wallace, J. J. Bellucci, A. Simonetti, T. Hainley, E. C. Koeman, and P. C. Burns, "A multi-method approach for determination of radionuclide distribution in trinitite," *Journal of Radioanalytical and Nuclear Chemistry*, vol. 298, no. 2, pp. 993–1003, Apr. 2013. [Online]. Available: http://link.springer.com/10.1007/s10967-013-2497-8 33, 46, 59

[21] S. D. Harvey, M. Liezers, K. C. Antolick, B. J. Garcia, L. E. Sweet, A. J. Carman, and G. C. Eiden, "Porous chromatographic materials as substrates for preparing synthetic nuclear explosion debris particles," *Journal of Radioanalytical and Nuclear Chemistry*, vol. 298, no. 3, pp. 1885–1898, Jun. 2013. [Online]. Available: http://link.springer.com/10.1007/s10967-013-2563-2 37

[22] H.-C. Chuang, W.-S. Hwang, and S.-H. Liu, "Effects of Basicity and FeO Content on the Softening and Melting Temperatures of the CaO-SiO2-MgO-Al2O3 Slag System," *Materials Transactions*, vol. 50, no. 6, pp. 1448–1456,

2009. [Online]. Available: http://joi.jlc.jst.go.jp/JST.JSTAGE/matertrans/MRA2008372?from=CrossRef 37

[23] J. B. Hanni, E. Pressly, J. V. Crum, K. B. C. Minister, D. Tran, P. Hrma, and J. D. Vienna, "Liquidus temperature measurements for modeling oxide glass systems relevant to nuclear waste vitrification," *Journal of Materials Research*, vol. 20, no. 12, pp. 3346–3357, 2005. 37

[24] A. Fluegel, "Modeling of Glass Liquidus Temperatures using Disconnected Peak Functions," 2007. [Online]. Available: http://glassproperties.com/liquidus/ 40

[25] S. Sukenaga, N. Saito, K. Kawakami, and K. Nakashima, "Viscosities of CaOSiO2Al2O3(R2O or RO) Melts," *ISIJ International*, vol. 46, no. 3, pp. 352–358, 2006. 40

[26] J. D. Vienna, P. Hrma, J. V. Crum, and M. Mika, "Liquidus temperature - composition model for multi-component glasses in the Fe , Cr , Ni , and Mn spinel primary phase field," *Journal of Non-Crystalline Solids*, vol. 292, pp. 1–24, 2001. 40

[27] Q. Rao, G. F. Piepel, P. Hrma, and J. V. Crum, "Liquidus temperatures of HLW glasses with zirconium-containing primary crystalline phases," *Journal of Non-Crystalline Solids*, vol. 220, no. 1, pp. 17–29, Oct. 1997. [Online]. Available: http://linkinghub.elsevier.com/retrieve/pii/S0022309397002275 40

[28] T. M. Semkow, P. P. Parekh, and D. K. Haines, "Modeling the Effects of the Trinity Test," in *Applied Modeling and Computations in Nuclear Science*, T. M. Semkow, S. Pomme, S. M. Jerome, and D. J. Strom, Eds. American Chemical Society, 2007, pp. 142–159. 42

[29] IAEA, *IAEA Safeguards Glossary*, 2001st ed. Vienna, Austria: IAEA, 2001, no. 3. 44

[30] R. Serber, *Los Alamos Primer*, R. Serber and R. Rhodes, Eds. Los Angelas: University of California Press, 1943. 45

[31] H. G. Norment, *DELFIC: Department of Defense Fallout Prediction System, Volume 1 - Fundamentals*. Defense Nuclear Agency, 1980. 45

[32] S. Hartland and R. J. Nesbitt, "Thermal Decomposition of Uranyl Nitrate Hexahydrate," *Journal of Applied Chemistry*, vol. 14, no. 9, pp. 406–412, 1964. 47

[33] B. Mason, "Lunar Tridymite and Cristobalite," *American Mineralogist*, vol. 57, pp. 1530–1535, 1972. 59

Vita

Joshua Molgaard is an Army Officer with eight years of military service. He also holds an M. S. in Physics from Clemson Univeristy. He has worked as an intern for Westinghouse TRU Solutions in support of the Waste Isolation Pilot Plant (WIPP) in Carlsbad, New Mexico, and also at Lawrence Livermore National Laboratory (LLNL). His military service includes a deployment to Iraq in 2007 and a two year stint in Consequence Management with the 4th Maneuver Enhancement Brigade. He has been selected to serve as an instructor at the United States Military Academy (USMA) at West Point beginning in 2014.